BRNO UNIVERSITY OF TECHNOLOGY

VYSOKÉ UČENÍ TECHNICKÉ V BRNĚ

FACULTY OF MECHANICAL ENGINEERING

FAKULTA STROJNÍHO INŽENÝRSTVÍ

ENERGY INSTITUTE

ENERGETICKÝ ÚSTAV

PERISTALTIC PUMP

PERISTALTICKÉ ČERPADLO

MASTER'S THESIS

DIPLOMOVÁ PRÁCE

AUTHOR — Bc. Radim Burda

AUTOR PRÁCE

SUPERVISOR — prof. Ing. František Pochylý, CSc.

VEDOUCÍ PRÁCE

BRNO 2019

VYSOKÉ UČENÍ TECHNICKÉ V BRNĚ
FAKULTA STROJNÍHO INŽENÝRSTVÍ

Zadání diplomové práce

Ústav:	Energetický ústav
Student:	**Bc. Radim Burda**
Studijní program:	Strojní inženýrství
Studijní obor:	Fluidní inženýrství
Vedoucí práce:	**prof. Ing. František Pochylý, CSc.**
Akademický rok:	2018/19

Ředitel ústavu Vám v souladu se zákonem č. 111/1998 o vysokých školách a se Studijním a zkušebním řádem VUT v Brně určuje následující téma diplomové práce:

Peristaltické čerpadlo

Stručná charakteristika problematiky úkolu:

Diplomová práce bude zaměřena na návrh peristaltického čerpadla s ohledem na snížení tlakových pulzací a hodnoty smykových napětí.
Bude navržena úplná konstrukce čerpadla, včetně kladek a pohonu.

Cíle diplomové práce:

Tvorba matematického modelu tlakových pulzací.
Výpočtové modelování proudění kapaliny v pružné trubici.
Návrh konstrukce peristaltického čerpadla.
Návrh motoru.
Výroba dílů na 3D tiskárně.
Odměření charakteristiky čerpadla.

Seznam doporučené literatury:

CENGEL, Yunus A. a John M. CIMBALA. Fluid mechanics: fundamentals and applications. 2nd ed. Boston: McGraw-Hill Higher Education, c2010. ISBN 00-772-9546-3.

BRDIČKA, Miroslav. Mechanika kontinua. Praha: Československá akademie věd, 1959. Úvod do teoretické fysiky.

Termín odevzdání diplomové práce je stanoven časovým plánem akademického roku 2018/19.

V Brně, dne 25. 10. 2018

doc. Ing. Jiří Pospíšil, Ph.D.
ředitel ústavu

doc. Ing. Jaroslav Katolický, Ph.D.
děkan fakulty

Abstract

The purpose of this thesis is to design peristaltic pump for a hemodialysis unit, with emphasis on minimization of pressure pulses. Through analytical analysis, a new concept for reduction of pressure pulses, that uses acceleration to increase pressure in volume between rollers, is devised. The operation of peristaltic pump is simulated via Ansys Fluent to get a better understanding of the flow inside the pump. Parallel to the new concept, a more traditional pump is designed, manufactured and experimentally tested to obtain information that can be used for the new concept.

Keywords

Peristaltic pump, hemodialysis, renal replacement, pressure pulsation, dynamic mesh, tygon.

Abstrakt

Cílem této diplomové práce je navrhnout peristaltické čerpadlo pro hemodialýzu s ohledem na minimalizaci tlakových pulzací. Pomocí analytické analýzy je navržen nový koncept redukce tlakových pulzací, který využívá zrychlení k navýšení tlaku v prostoru mezi válečky. Fungování peristaltického čerpadla je simulováno pomocí programu Ansys Fluent pro získání lepší představy o proudění v čerpadle. Souběžně s návrhem nového konceptu bylo navrženo více tradiční čerpadlo, které bylo následně vyrobeno a experimentálně odzkoušeno. Data získaná z experimentu mohou být dále použita pro nový koncept.

Klíčová slova

Peristaltické čerpadlo, hemodialýza, náhrada funkce ledvin, tlakové pulzace, dynamická mesh, tygon.

BURDA, Radim. *Peristaltic pump.* Brno, 2019. Master's thesis. Brno University of Technology, Faculty of Mechanical Engineering, Energy institute. Supervisor František Pochylý.

BURDA, Radim. *Peristaltické čerpadlo*. Brno, 2019. Diplomová práce. Vysoké učení technické v Brně, Fakulta strojního inženýrství, Energetický ústav. Vedoucí práce František Pochylý.

Declaration

I declare that I have personally elaborated the master's thesis *Peristaltic pump* independently, under the supervisor prof. Ing. František Pochylý, CSc., using the sources which are all listed in the bibliography section.

Brno, May 24, 2019 ……

Radim BURDA

I would like to express deep gratitude to my supervisor prof. Ing. František Pochylý, CSc. for numerous valuable suggestions, as well as steady support and welcoming attitude.

I highly appreciate advice from Ing. Roman Klas, Ph.D. and Ing. Dominik Šedivý on simulations with dynamic mesh. Furthermore, I would like to thank Ing. Martin Hudec, Bronislav Kusý and Karel Večera for valuable comments considering the design of peristaltic pump, as well as invaluable support during experimental part of the thesis.

Last paragraph belongs to my family, friends and loved ones for continuous and unparalleled support and encouragement not only throughout the studies, but also in my personal life. Special recognition belongs to Yveta Jarošíková for being so awesome.

Table of contents

1. Introduction

In case of kidney disease or failure the patient requires other means to extract superfluous waste from their body. The most advantageous solution is a renal transplant which demonstrates the best results from the medical point of view [1] as well as being the most pleasant and cheap option for the patient. However, the demand for kidney transplant is much higher than the supply which means that patient can wait for the transplant for years [2][3]. The patients, "stuck" on the waiting list or unable to receive a transplant due to a medical condition, have to rely on artificial renal replacements - most notably peritoneal dialysis, hemofiltration or hemodialysis.

The most widely used method is hemodialysis which uses filtration through semipermeable membrane to transfer unwanted particles from blood to dialysate on the other side of the membrane. The improvement of hemodialysis is an important subject of research as the numbers of patients with end stage kidney disease (ESKD) are progressively increasing and the demand for hemodialysis is raising [4]. While it is most important to focus on the component responsible for waste removing process – the dialyzer – it is also crucial to improve other components of the hemodialysis unit that contribute to effectiveness of the entire system.

In this thesis, the focus is on the component responsible for pressure and flow rate in the system – the blood pump. While there are many types of blood pumps used in renal replacement therapies, the most common is a peristaltic pump which uses rollers attached to a rotor to compress a flexible tube to propel blood through the system. Peristaltic pumps are often associated with oscillating flow rate which results in pressure pulses, especially during compression and decompression of the tube, caused by reflux as the pressure difference in front of and behind the roller stabilizes. The pressure pulses may lead to deformation of blood cells [5] and it is therefore necessary to optimize the pump to achieve pressure course as stable as possible.

The main objective of this thesis is to investigate blood flow during the operation of peristaltic pump by analytical analysis and numerical simulations and, based on the obtained information, design an optimal peristaltic pump with emphasis on reduction of the pressure pulses during compression and decompression of the flexible tube.

The second and the third chapter are devoted to a brief introduction to renal replacement, with emphasis on hemodialysis, and peristaltic pumps, primarily focused on design recommendations. The fourth chapter is focused on governing equations which are used for derivation of force equation describing the peristaltic movement. The following chapter is then dedicated to two designs of a peristaltic pump – the first "basic" design and the second design that uses acceleration of the second roller to reduce pressure pulses. The sixth chapter describes numerical simulations, with emphasis on wall deformation using dynamic mesh. In the last chapter, the experimental analysis of the first "basic" design is carried out to confirm the correctness of the numerical simulations.

2. Renal replacement

The following chapter provides a brief introduction to the functions of human kidney, its importance and issues connected with kidney disease or failure. Proper understanding of difficulties that patients have to endure can provide motivation as well as valuable information that can be utilized during the developing process. The organs of human body can be seen as machines, optimized through thousands of years of evolution, that serve as an imaginary end goal of human invention.

The first part of the chapter describes the physiology of human kidney and outlines its differences to accessible artificial replacements. The following part expands on this subject by providing a list of possible replacement therapies with emphasis on hemodialysis while highlighting the benefits of human transplantation and issues connected to the shortage of donors.

2.1 Human kidney

The human kidney is an important organ as it provides numerous functions which maintain a healthy balance inside the human body. The primary function of kidney is to balance the solutes in the body, but it is also accountable for secreting hormones which contributes to regulation of homeostasis. [6]

Nephron, a basic unit of human kidney, is responsible for three main functions that regulate the solute in the human blood – filtration, reabsorption and secretion. The nephron consists of 5 parts:

- Bowman's capsule (also known as renal corpuscle)
- proximal tubule
- loop of Henle
- distal tubule
- and collecting ducts. [7]

Approximately 625 ml of plasma flows through each kidney every minute. Around 20 % of these 625 ml (which corresponds to 125 ml) is filtered across the glomerulus. However, due to reabsorption and secretion, only 1 ml of urine is excreted into bladder every minute because the human kidney reabsorbs substances that are beneficial for homeostasis. For example, all glucose is filtered in renal corpuscle and then immediately reabsorbed in the proximal tubule as it is beneficial to the homeostasis [6]. The waste removal process of human kidney can be seen in Figure 1.

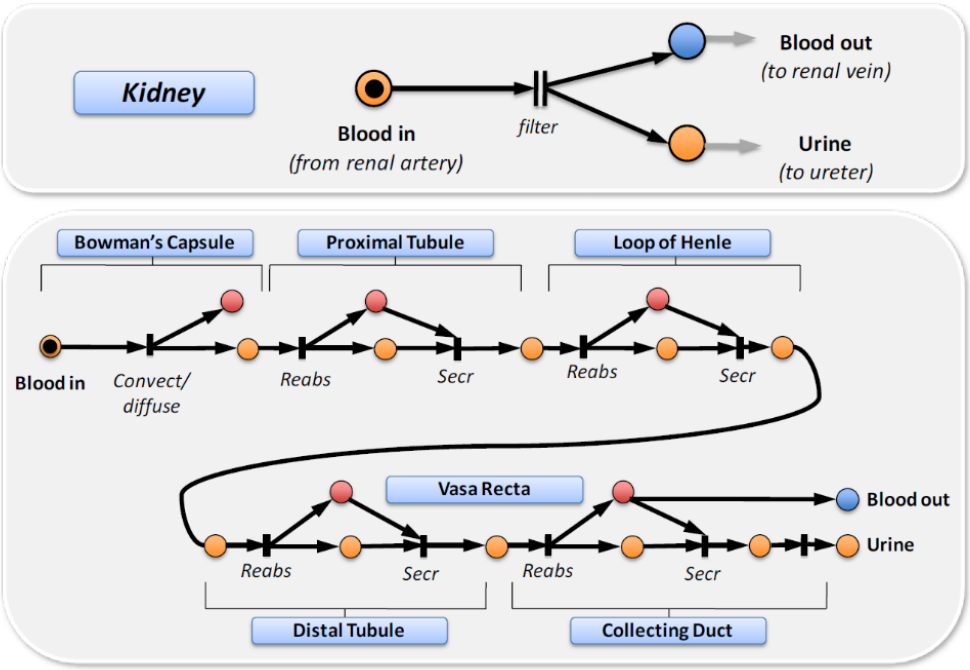

Figure 1 – Basic functionality of human kidney (top), detailed model of waste removal (bottom) [6]

There are two most notable differences in the functioning of human kidney and most artificial replacements [6]:

- Human kidney uses thousands of small identical functional units (nephrons) instead of one large unit.
- It uses multi-step filtration process.

The use of many small units instead of a large unit can be also found in various other biological systems. This approach grants a small output unit a possibility to produce big results on a larger scale. Similar approach can be also found in industrial setting (for example solar arrays). While this way can be incorporate into the design, basically all the pumps on the market function as one large unit.

The multi-step filtration (kidney removes both desirable and undesirable solutes and then reabsorbs the desirable ones back into the system) provides the opportunity for specialized molecule removal with the drawback that large amount of removed fluids from the blood must be replaced. Similar process is reproduced in hemofiltration but due to the drawback it is reserved for patients in intensive care. Typical hemodialysis system uses one step filtration where the undesirable particles are filtrated from the blood in a dialyzer and desirable solutes are absorbed back from dialysate.

2.2 Current renal replacement therapies

In case of kidney disease or failure (also called nephropathy) the patient requires an external device which will remove waste from the body. The most suitable solution is renal transplant since it is the cheapest option and the option with the best prognosis for the patient. Most notably patients who are from 20 to 39 years old, while placed on the waiting list and then undergo the transplantation, are projected to live almost 17 years longer than the patients who then did not receive transplantation [1]. It is also worth noting that with proper procedure the life expectancy of kidney donors is very similar to normal population [8].

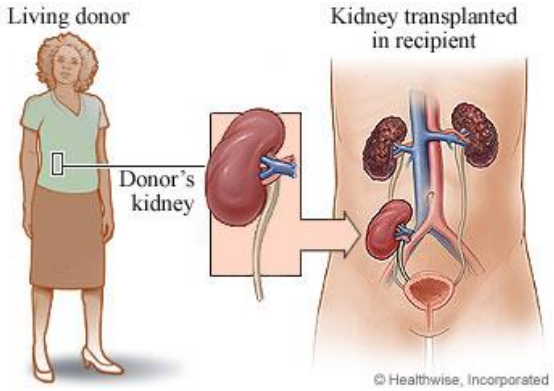

Figure 2 – Location of transplanted kidney [9]

However, the demand for kidneys is much higher than the offer. For example, in 2009 in Switzerland the average waiting time was 700 days [2]. In 2006 in the Czech Republic only 395 out of 4738 (8,33%) [3] patients attending dialysis received a renal transplant (however this number also includes the patients who are not suited for renal transplant). High demand for kidneys may even result in formation of an illegal market especially in the developing world [10]. Due to the long waiting time the patient is placed on the waiting list and has to attend dialysis while waiting for the suitable donor. The dialysis is often regarded as "holding measure" but can also be the only option as the patient can be unsuitable for transplant.

The main problem with dialysis is that the patient is typically required to attend hospital three times per week with 4 h for each session. In addition, the required amount of dialysate is around 120 l for each session which is one of the reasons why the treatment is typically related to high cost (for example in Switzerland 80 000 euros per patient per year) [2].

While on the waiting list the patient has three main options:

- peritoneal dialysis
- hemodialysis
- hemofiltration

Peritoneal dialysis is usually the first method of treatment reserved for patients with not so severe conditions. Peritoneal dialysis functions the same way as traditional dialysis but uses peritoneal membrane surrounding the abdomen as a filter. As this method can be performed by

the patient himself, there is no reliance on hospital's schedule. However, the peritoneal dialysis must be done several times a day while traditional dialysis requires only few hours per day. Additionally, the membrane's ability to filtrate is reduced after several years of treatment and peritoneal dialysis is linked to more negative effects on human body than hemodialysis performed in hospital. In most cases the patients undergoing the peritoneal dialysis switch to hemodialysis after a couple of years [6].

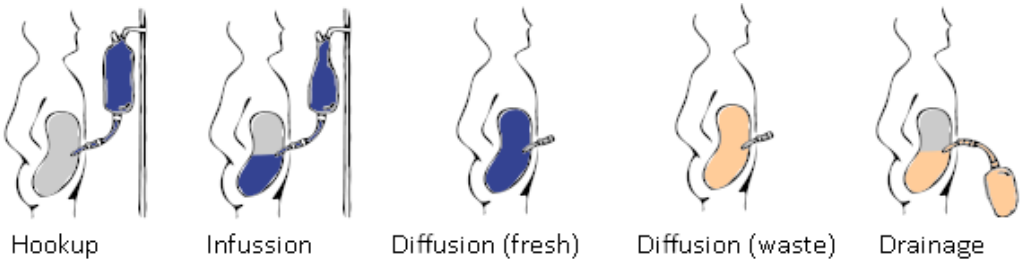

Figure 3 – Peritoneal dialysis process [11] (Edited)

Hemofiltration is recognized as a form of renal-replacement therapy in acute renal failures. While having many similarities with hemodialysis, it resembles the filtration process of the human kidney more closely. The membrane is more permeable than the one used for hemodialysis and therefore allows both water and substance up to molecular weight of about 20 000 to pass through the membrane. Unlike in human kidney, the filtrate is then discarded, and the patient receives an infusion of necessary solution. Therefore, hemofiltration can be seen as a process similar to secretion followed by reabsorption. [12]

2.2.1 Hemodialysis

The main objective of hemodialysis is to remove solutes (sodium, potassium, urea, etc.) that have accumulated due to renal failure. Approximately 1,5 – 4,5 liters of water needs to be removed during each treatment. In general, during the treatment the blood enters the extracorporeal circuit and is then led by blood pump through artificial kidney where the blood is cleaned from undesired solute and then exits back to the patient. Counter direction to the blood flow is the dialysate which absorbs undesired particles and is then disposed of or, in some cases, regenerated for multiple uses (each regeneration drops the efficiency of the filtering) [6][11]. Simplified function of the artificial kidney can be seen in Figure 4.

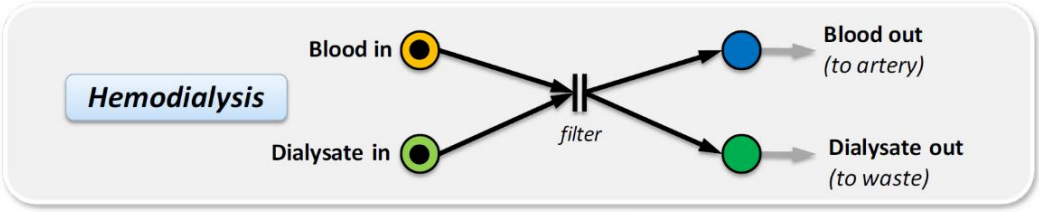

Figure 4 – Simplified function of hemodialysis [6]

The blood accesses the extracorporeal circuit through either intravenous catheter, arteriovenous fistula (AV) or synthetic graft. The type of access depends on various factors such as the condition of patient's vasculature, expected time course of patient's renal failure etc. The pressure behind the access is around -100 mmHg (relative to atmospheric pressure)[1] [13][14]. The blood then continues through the blood pump, which covers all the pressure losses in the system[2], to the dialyzer.

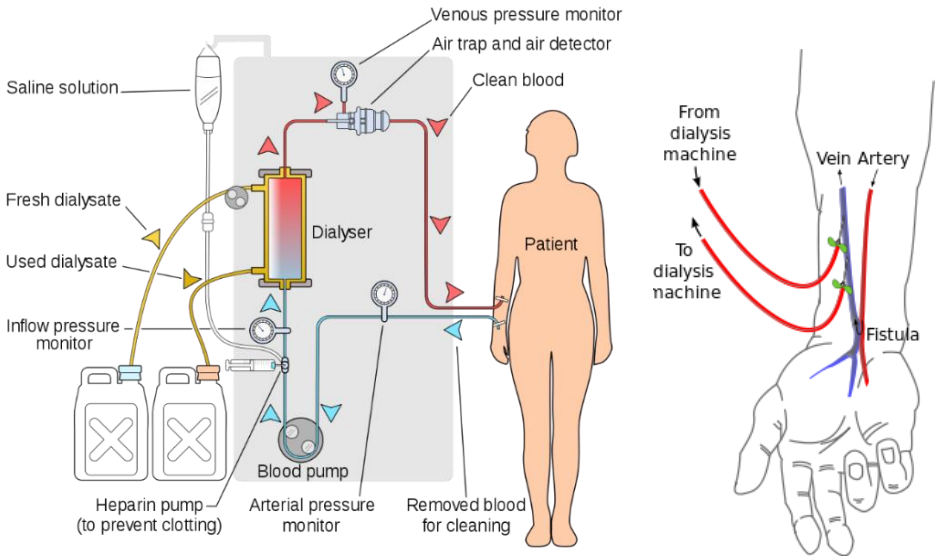

Figure 5 – Hemodialysis schematic (left), vascular access (right) [11] (edited)

In the dialyzer the dialysate and blood are separated by semi-permeable membrane and therefore the fluids are not in direct contact. The membrane is permeable only for very small particles (approximately up to 60 Daltons) whereas larger particles such as blood cells remain in the blood [12]. During the first dialysis trials the membrane was created from animal membranes (fish bladder, intestine, etc.), whereas now artificial materials are used (cellophane, glucose esters or cuprophan). Unfortunately, the artificial materials can stimulate the immune system of the patient which can result in higher risk of rejection of the transplant in the future [11].

The blood flow in the dialyzer is laminar with flow rate at around 200-350 ml/min. The laminar flow is important as the red blood cells are grouped in the middle of the stream and are surrounded by the plasma. This configuration provides protection for the blood cells while having plasma located near the surface helps with the filtration as most of the unwanted particles are located in the plasma. On the other hand, the flow of the dialysate is turbulent with flow rate at around 500 ml/min. Turbulent flow helps the filtration as well [11]. When blood and dialysate flow through the dialyzer, a concentration gradient is formed as the concentration of solute in the blood is different than the concentration in the dialysate which results in the

[1] Detailed overview of pressure during the whole hemodialysis can be found in chapter 5.1
[2] More information about the blood pumps can be found in the chapter 3

movement of the water across the membrane from intravascular space to the dialysate compartment. The solutes are then dragged with the water.

Blood then reenters the intracorporeal system with pressure around 80 mmHg (relative to atmospheric pressure) [14]. Considering that blood comes into contact with different materials than endothelium of blood vessels (surface of blood vessels), the danger of thrombosis (blood clotting) must be taken into consideration. Due to this danger the patient is usually heparinized. Also, the circuit is usually supplied with an air detector because the presence of air bubbles can lead to embolization (the vessels get blocked by the air bubble which can result in insufficient blood supply to the referred area). Air in bloodlines can occur due to the underfilled air trap chamber, inadequate priming, loose connections, empty saline bag, or dialysis needle dislodgement/removal while the blood pump is still running [15].

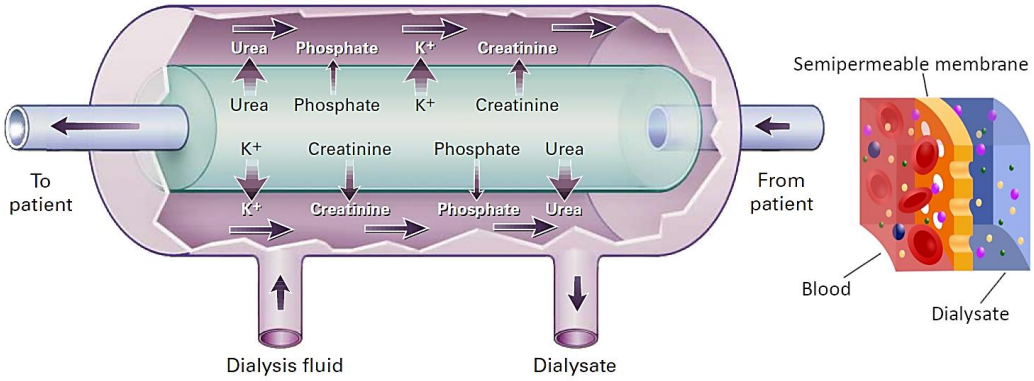

Figure 6 – Dialyzer with semipermeable membrane [12] (edited)

3. Rotary peristaltic pumps

This chapter is devoted to a brief introduction of rotary peristaltic pumps. While the working principle of peristaltic pumps can be applied to different setups, the most widely used setup is the rotary peristaltic pump. The rotary peristaltic pump was invented in 1932, yet it still plays a crucial part in medical field to this day.

In the first part of the chapter, the working principle of peristaltic pumps is introduced, as well as key parameters that need to be taken into consideration during the designing process. The second part provides a summary of recommendations to prevent pump-induced hemolysis.

3.1. Working principle and key parameters

Following chapter is composed based on the following sources [16][17][18]. The working principle of peristaltic pump is relatively simple. The pump utilizes the concept used in many biological systems (gastrointestinal tract, etc.) – the peristaltic movement. The fluid is contained within a flexible tube by rollers attached to the rotor of the pump. As the rotor turns, the tube is periodically compressed and decompressed. The part under the compression closes, trapping the fluid in the volume between the rollers, thus forcing the fluid to be pumped through the tube alongside the pump. At the outlet the tube is decompressed, therefore letting the fluid continue to the circuit. As the tube restitutes to its natural shape after being passed by the roller, arising negative pressure leads to suction of more fluid into the pump. This means that peristaltic pumps are self-priming.

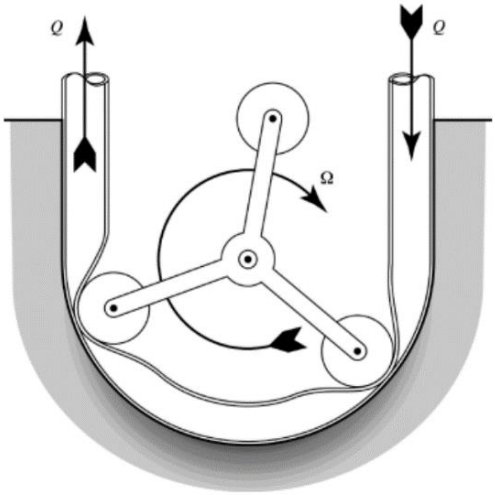

Figure 7 – Scheme of peristaltic pump with 3 rollers [19]

Figure 8 – Peristaltic pump [20]

When designing peristaltic pump there are some key features that have to be taken into consideration:

1. **Pump rpm (revolutions per minute):** Considering the tube is periodically decompressed during the operation, the tube has to be created from a resistant material that will withstand the periodic cycle. Not taking the material into consideration, the lifespan of the tubing is dependent on number of rollers and pump rpm. The lifespan of tubing is not the most important factor for hemodialysis, as tubing is commonly replaced with each patient, but is an important factor when the replacement can be difficult – for example in chemical industry.
2. **The material of tubing:** As the tube is the only part that comes into contact with the fluid, the material is very important. Besides its strength properties, the material has to be able to withstand aggressive fluids transported in chemical industry. In the medical field the material has to be nonreactive with blood, so blood of the patient does not get contaminated.
3. **Occlusion settings:** Occlusion means the gap between the roller and the casing and determines the squeeze applied to the tube. More squeeze decreases the lifespan of the tube while more open occlusion can lead to reversed flow (especially for high pressure pumping), which leads to dramatic drop in efficiency. High occlusion can even lead to spallation of particles from the tube to fluid which in medical field can result in blood contamination [21]. Occlusion is a function of wall thickness and not the inner diameter, therefore it is common to use tubes with more than one value of inner diameter while maintaining the same occlusion.

3.2 Design recommendation

The operation of extracorporeal circuit comes with inevitable risk of blood damage. Most notably the danger of hemolysis, blood loss or embolism. The blood cells come into contact with a foreign object and mechanical shear which has negative effect on the lifespan of erythrocytes [21]. In comparison to the other components of a hemodialysis unit, the peristaltic pump is not regarded as a main source of hemolysis. Therefore, reduced effort was devoted to the measurements of pump-induced hemolysis in this field [21].

Knight (1973) describes the four basic fluid mechanical effects generally occurring in peristaltic pumps which may have damaging influence upon blood cells [5]:

1. velocity gradients, which cause a shearing effect between adjacent fluid layers
2. pressure variations which may lead to cell deformation
3. flow stagnation
4. turbulent flow which enhances the rate at which fresh elements of blood are brought into contact with a flow obstruction

All four effects may occur in peristaltic blood pump, most notably during the compression and decompression of the tube. During the sudden decompression the pressure in front of and behind the leading roller equalizes which results in a reversed flow. The reverse flow causes sudden pressure rise which, as stated before, may result in blood cell deformation. The oscillating flow rate is not in itself connected with any damage to the cells but may cause pain and discomfort to the patient. The oscillating course of pressure during hemodialysis can be seen in Figure 9.

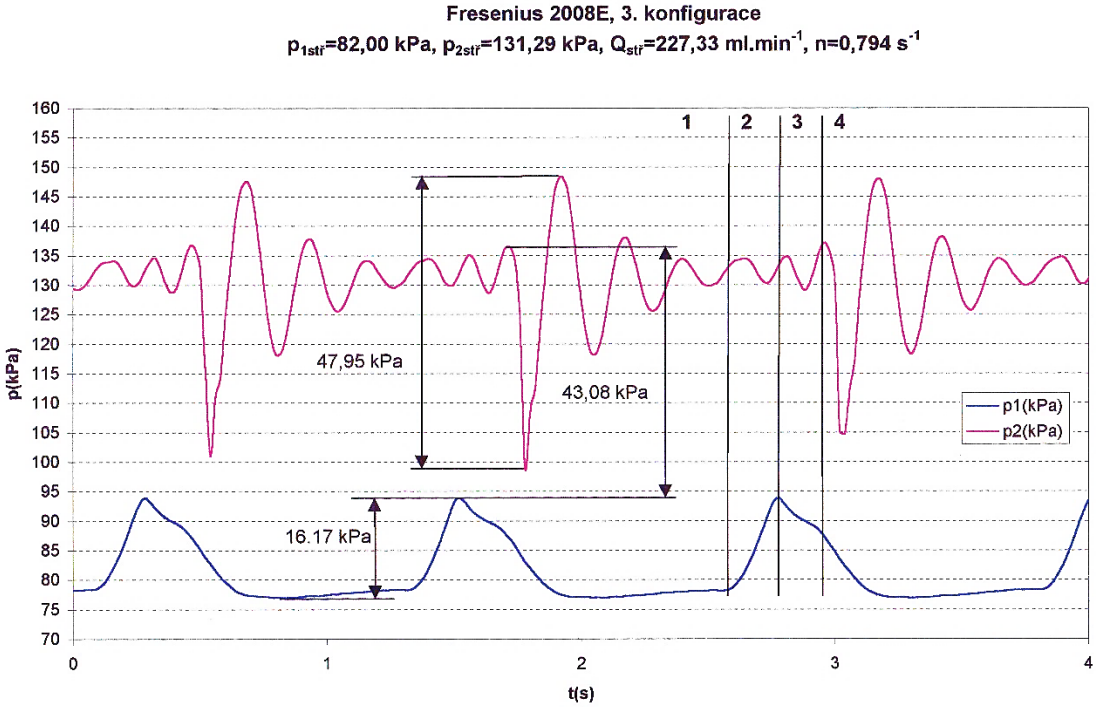

Figure 9 – Pressure course in front (p_1) and behind (p_2) the peristaltic pump during hemodialysis treatment [22]

As stated before, little effort has been devoted to the measurement of pump-induced hemolysis, but some recommendation for the design of peristaltic pump can be obtained. Researchers agree that hemolysis decreases with increasing roller and tube diameter and also with more opened occlusion [21][23]. While all three of these parameters are major variables governing the hemolysis, they contribute to the presence or absence of hemolysis independently as no optimal geometry or ratio of sizes was discovered to minimize blood trauma [21]. Lastly, the hemolysis seems to be independent of the number of rollers, and more than two rollers are less likely to trap air during the priming [21].

4. Governing equations

In order to design the best possible pump, it is necessary to understand the equations behind the flow in the deforming tube of the pump. A full analytical solution is often not possible, but a partial solution using convenient simplifications can provide useful information for the designing process. Firstly, the most important equations describing the fluid movement through the pump are introduced – Navier-Stokes equations and Continuity equation. Then, the peristaltic pump movement is analysed through the force equation derived from Navier-Stokes equations. This analysis can provide practical information about the effect of the force applied to the tube by the roller of the pump which can be used to further improve the design.

4.1 Navier-Stokes equations

By applying Newton's second law to fluid motion we get the Navier-Stokes equations which describe the motion of viscous fluids. The next description of the equations in fluid dynamics was written based on the lectures of prof. Pochylý as well as a variety of other sources [24][25][26]. The Navier-Stokes equations can be described as follows:

$$\rho \frac{\partial v_i}{\partial t} + \rho \frac{\partial v_i}{\partial x_j} v_j - \frac{\partial \sigma_{ij}}{\partial x_j} = \rho g_i \tag{1}$$

where ρ is the density of the fluid; v_i, v_j are velocity vectors; t is time; x_i , x_j are coordinates of the volume; g_i is the vector of the gravitational acceleration and σ_{ij} is the stress tensor. The stress tensor can be specified:

$$\sigma_{ij} = \pi_{ij} + \tau_{ij} \tag{2}$$

where

$$\pi_{ij} = 2\eta v_{ij} + \delta_{ij} b v_{kk};\ \tau_{ij} = \delta_{ij} p. \tag{3)(4}$$

The π_{ij} is viscous stress tensor, τ_{ij} is tensor of mechanical pressure, η is dynamic viscosity, v_{ij} is rate-of-strain tensor, δ_{ij} is the Kronecker tensor, b is second viscosity (also known as volume viscosity), v_{kk} is divergence of velocity and p is pressure. In practice, the viscosity coefficient changes with temperature, however we take η as a constant. Furthermore, for incompressible fluids the second viscosity is superfluous as the v_{kk} equals zero. This means the stress tensor represents the impact of pressure and viscosity.

4.2 Continuity equation

The continuity equation states that the rate at which mass enters the system is equal to the rate at which mass leaves the system plus the accumulation of mass within the system. The equation can be written in differential form as follows [25] [27] [26]:

$$\frac{\partial \rho}{\partial t} + \frac{\partial}{\partial x_i}(\rho v_i) = 0 \tag{5}$$

If the flow is approximated as incompressible and density is not a function of time or space, the equation can be transformed to the incompressible continuity equation:

$$\frac{\partial v_i}{\partial x_i} = 0 \tag{6}$$

4.3 Derivation of the force from Navier-Stokes equations

To determine the impact of the force, effecting the rubber tube, on the fluid in the peristaltic pump it is first necessary to derivate the force equation from Navier-Stokes equation. After the derivation it is possible to adapt the equation to correspond the compression occurring in the peristaltic pump.

Following derivation was done based on the lectures of Fluid Engineering and Fluid Structure Interaction lectured by prof. Pochylý as well as course book written by prof. Pochylý [25] [28].

Derivation starts with Navier-Stokes equation:

$$\rho \frac{\partial v_i}{\partial t} + \rho \frac{\partial v_i}{\partial x_j} v_j - \frac{\partial \sigma_{ij}}{\partial x_j} = \rho g_i \tag{7}$$

Considering incompressible fluid and fluid with constant density we can apply these simplifications to the Navier-Stokes equation. These simplifications are vital as we are now able to use Gaus-Ostrogradsky equation to transform volume integral to surface integral which is advantageous considering it is easier to acquire data of velocity and pressure only from the surface of the volume than from the entire volume. The prove of these simplifications can be seen in the appendix.

$$\rho g_i = \frac{\partial}{\partial x_j}\left(\delta_{ij} \rho g_l x_l\right);\ \frac{\partial v_i}{\partial x_j} v_j = \frac{\partial}{\partial x_j}\left(v_i v_j\right);\ \frac{\partial v_i}{\partial t} = \frac{\partial}{\partial x_j}\left(\frac{\partial v_j}{\partial t} x_i\right) \tag{8)(9)(10}$$

By applying these simplifications to the equation (7) we get:

$$\rho \frac{\partial}{\partial x_j}\left(\frac{\partial v_j}{\partial t} x_i\right) + \rho \frac{\partial}{\partial x_j}\left(v_i v_j\right) - \frac{\partial \sigma_{ij}}{\partial x_j} - \frac{\partial}{\partial x_i}\left(\rho g_j x_j\right) = 0. \tag{11}$$

The equation above represents the force on volume equal to 1 m^3. To determine the total force in the entire volume, the equation needs to be multiplied by volume element dV and integrated over the whole volume V. Because of the simplifications it is now possible to apply Gaus-Ostrogradsky's equation. After these operations we get the following equation:

$$\int_{\theta=\Gamma\cup S} \left(\rho \frac{\partial v_j}{\partial t} x_i + \rho\left(v_i v_j\right) - \left(\rho g_j x_j\right)\right) n_j d\theta - \int_S \sigma_{ij} n_j dS - \int_\Gamma \sigma_{ij} n_j d\Gamma = 0. \tag{12}$$

The force of the fluid effecting the solid (see Figure 10 and Figure 11) consists of the viscous and pressure component (see Chapter 4.1) and is described by the equation:

$$F_i = -\int_S \sigma_{ij} n_j dS. \tag{13}$$

Applying the definition of the force effecting the solid in the fluid on the equation x we get the final form of the equation:

$$F_i = \int_{\theta=\Gamma\cup S} \left(\rho \frac{\partial v_j}{\partial t} x_i + \rho(v_i v_j) - (\rho g_j x_j) \right) n_j d\theta - \int_\Gamma \sigma_{ij} n_j d\Gamma. \tag{14}$$

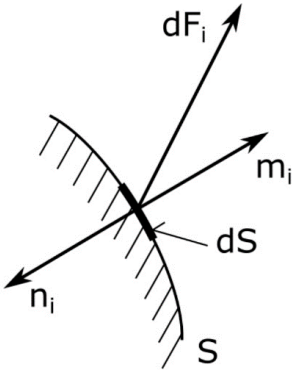

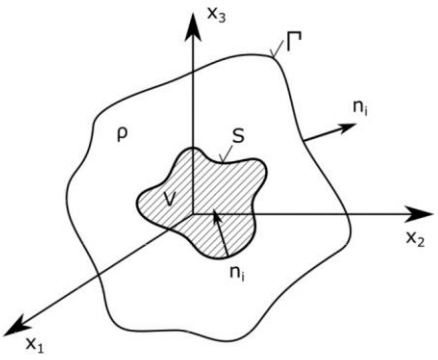

Figure 10 – Force on surface element (left) [24]

Figure 11 – Solid body in closed volume of fluid (right) [24]

4.3.1 Analysis of peristaltic pump movement

The force equation can be applied to the peristaltic pump movement – specifically how the force applied to tygon tube effects the characteristics and movement of the fluid inside the said tube. A complete analytical solution is not possible because the issue is far too complicated, but through analytical analysis it is possible to get better understanding of the flow inside the tube. With appropriate simplification we can predict the impact of various components of the equation, especially during the time independent motion, and based on these predictions design a superior peristaltic pump which would reduce the pressure pulsation and shear.

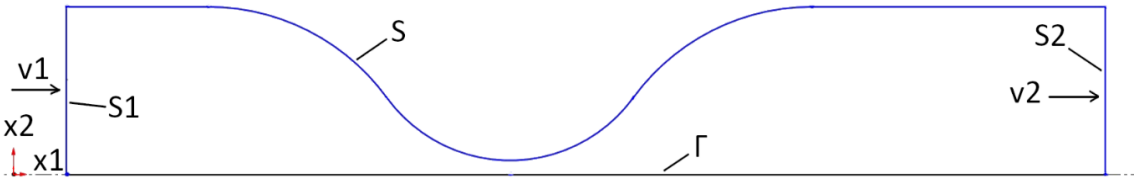

Figure 12 – Analysis of peristaltic movement

The equation (14) can be transformed to correspond with Figure 12. In order to be able to analyse the equation it is necessary to simplify it first. Also, the assumptions used for derivation of the force equation in the previous chapter are reminded:

- The gravitation component is insignificant in comparison to the other components of the equation → $g_j = 0$
- Incompressible fluid and constant density → $\frac{\partial v_i}{\partial x_j} = 0;\ \rho = constant$
- The tube is considered linear (the curvature is disregarded)
- Two-dimensional space ($i = 1,2$)

The force equation can be then written in the following form:

$$F_i = \int_{\Gamma \cup S} \sigma_{ij} n_j d\Gamma = \int_{\theta=\Gamma \cup S \cup S_1 \cup S_2} \left(\rho \frac{\partial v_j}{\partial t} x_i + \rho(v_i v_j) \right) n_j d\theta - \int_{\Phi=S_1 \cup S_2} \sigma_{ij} n_j d\Phi \tag{15}$$

After breaking down the equation (15) we can see the effect of all the components:

$$\begin{aligned} F_i = {} & \rho \int_{\Gamma} \frac{\partial v_j}{\partial t} x_i n_j d\Gamma + \rho \int_{S} \frac{\partial v_j}{\partial t} x_i n_j dS + \rho \int_{S_1} \frac{\partial v_j}{\partial t} x_i n_j dS_1 + \rho \int_{S_2} \frac{\partial v_j}{\partial t} x_i n_j dS_2 \\ & + \rho \int_{\Gamma} v_i v_j n_j d\Gamma + \rho \int_{S} v_i v_j n_j dS + \rho \int_{S_1} v_i v_j n_j dS_1 + \rho \int_{S_2} v_i v_j n_j dS_2 \\ & - \int_{S_1} \sigma_{ij} n_j dS_1 - \int_{S_2} \sigma_{ij} n_j dS_2. \end{aligned} \tag{16}$$

Since for a solid boundary, the velocity of the fluid must be equal to the velocity of the boundary (the no-slip condition adopted for a viscous fluid) and surface Γ is a stationary wall ($v = 0$),

$$\rho \int_{\Gamma} \frac{\partial v_j}{\partial t} x_i n_j d\Gamma = 0 \quad and \quad \rho \int_{\Gamma} v_i v_j n_j d\Gamma = 0. \tag{17) (18}$$

Then we shall specify the medium by taking the constitutive relation for a Newtonian viscous fluid,

$$\sigma_{ij} = \pi_{ij} - p\delta_{ij} = 2\eta v_{ij} - p\delta_{ij}. \tag{19}$$

Using $\delta_{ij} n_j = n_i$ the force equation can now be written as:

$$F_i = \rho \int_S \frac{\partial v_j}{\partial t} x_i n_j dS + \rho \int_{S_1} \frac{\partial v_j}{\partial t} x_i n_j dS_1 + \rho \int_{S_2} \frac{\partial v_j}{\partial t} x_i n_j dS_2 + \rho \int_S v_i v_j n_j dS$$
$$+ \rho \int_{S_1} v_i v_j n_j dS_1 + \rho \int_{S_2} v_i v_j n_j dS_2 - \int_{S_1} 2\eta v_{ij} n_j dS_1 - \int_{S_2} 2\eta v_{ij} n_j dS_2 \quad (20)$$
$$+ \int_{S_1} p n_i dS_1 + \int_{S_2} p n_i dS_2.$$

Equation (20) describes the impact of the force effecting the tube on the flow inside the tube. The components with integral over the surface S can be altered by the design of the pump as they represent the velocity and acceleration of the roller. This equation can be no longer simplified if we want to describe the deformation at the inlet and outlet of the pump where the effects in direction x_2 are not negligible. For the rest of the movement where the tube is already fully deformed, the equation can be simplified by the assumption that the roller is moving only alongside the tube (in direction x_1) and we can ignore the effects of the components of the equation in direction x_2, as they are likely inferior to the effects in direction x_1.

Applying this assumption to the equation (20), it can be written into following form:

$$F_1 = \rho \int_S \frac{\partial v_j}{\partial t} x_1 n_j dS + \rho \int_{S_1} \frac{\partial v_j}{\partial t} x_1 n_j dS_1 + \rho \int_{S_2} \frac{\partial v_j}{\partial t} x_1 n_j dS_2 + \rho \int_S v_1 v_j n_j dS$$
$$+ \rho \int_{S_1} v_1 v_j n_j dS_1 + \rho \int_{S_2} v_1 v_j n_j dS_2 - \int_{S_1} 2\eta v_{1j} n_j dS_1 \quad (21)$$
$$- \int_{S_2} 2\eta v_{1j} n_j dS_2 + \int_{S_1} p n_1 dS_1 - \int_{S_2} p n_1 dS_2.$$

This form of the equation can be modified by the following steps:

- For surface S_1:

$$x_1 = 0, v_j n_j = -v_1, p n_1 = -p \quad (22)$$

- For surface S_2:

$$x_1 = L, v_j n_j = v_1, p n_1 = p \quad (23)$$

- For surface S:

$$v_j n_j = v_n \quad (24)$$

- Viscous component for surface S_1, S_2:

$$v_{1j} n_j = v_{11} = \left(\frac{\partial v_1}{\partial x_1} + \frac{\partial v_1}{\partial x_1}\right) = 0 \Rightarrow 2\eta v_{1j} n_j dS_{1,2} = 0 \quad (25)$$

Using these modifications, the time dependent equation for direction x_1 now takes the final form:

$$F_1 = \rho \int_S \frac{\partial v_n}{\partial t} x_1 dS + \rho \int_{S_2} L \frac{\partial v_1}{\partial t} dS_2 + \rho \int_S v_1 v_n dS - \rho \int_{S_1} v_1^2 dS_1 + \rho \int_{S_2} v_1^2 dS_2 - \int_{S_1} p dS_1 + \int_{S_2} p dS_2 \tag{26}$$

and with further simplification time independent form:

$$F_1 = \rho \int_S v_1 v_n dS - \rho \int_{S_1} v_1^2 dS_1 + \rho \int_{S_2} v_1^2 dS_2 - \int_{S_1} p dS_1 + \int_{S_2} p dS_2. \tag{27}$$

The system of equations can be completed with continuity equation:

$$\int_S v_1 dS - \int_{S_1} v_1 dS + \int_{S_2} v_1 dS = 0. \tag{28}$$

4.3.2 Discussion

From equations (26), (28) we can now clearly see how the change in the velocity and acceleration of the roller directly effects the pressure and fluid velocity at the inlet and outlet of the pump (represented by surface S_1 and S_2).

Increasing the pressure by accelerating the roller can be especially helpful to increase the pressure in the volume between the two rollers. By doing so the flow reflux when the first roller exits the tube would be lower as the pressure difference between the pressure side and the suction side of the roller would be decreased. To achieve this, the second roller would have to be accelerated right after it fully compresses the tube and increase the pressure until the first roller fully exits the tube (see Figure 13). Unfortunately, this can be quite difficult as in the basic 180° concept the first roller starts to decompress the tube as soon as the second roller fully compresses the tube, so the second roller does not have enough time to increase the pressure enough.

The second roller could be accelerated rapidly to bypass this problem, but then we would likely face the pressure rise caused by this massive acceleration that could be harmful to the blood running through the tube. Secondly, the velocity of the roller during the compression and decompression of the tube should be as slow as possible as the sudden change can result in hydraulic shock which could be even more harmful to the blood cells.

In order to fully bypass this problem, it is necessary to differentiate from the basic 180° concept and opt for more unconventional 270° concept (see Figure 14) where the first roller decompresses the tube much later and the second roller compresses the tube sooner and therefore can accelerate more gradually. Generally, with longer time the second roller can travel

before the first roller exits the tube, the acceleration can be done more smoothly, and the volume between the roller can be pressurize more. The design can also be adjusted by using more than 2 rollers, but this possibility is not analysed as it is not the main focus of the thesis. For better understanding see Figure 14 where the difference between the trajectory length feasible for acceleration of the second roller can be seen.

While there are many possibilities how to achieve the acceleration of the second roller, the easiest one is to switch form a circular to the elliptical design of the pump. The distance between the center of the rotation and the roller would gradually increase and therefore the velocity of the roller would increase as well. More on this topic in the next chapters.

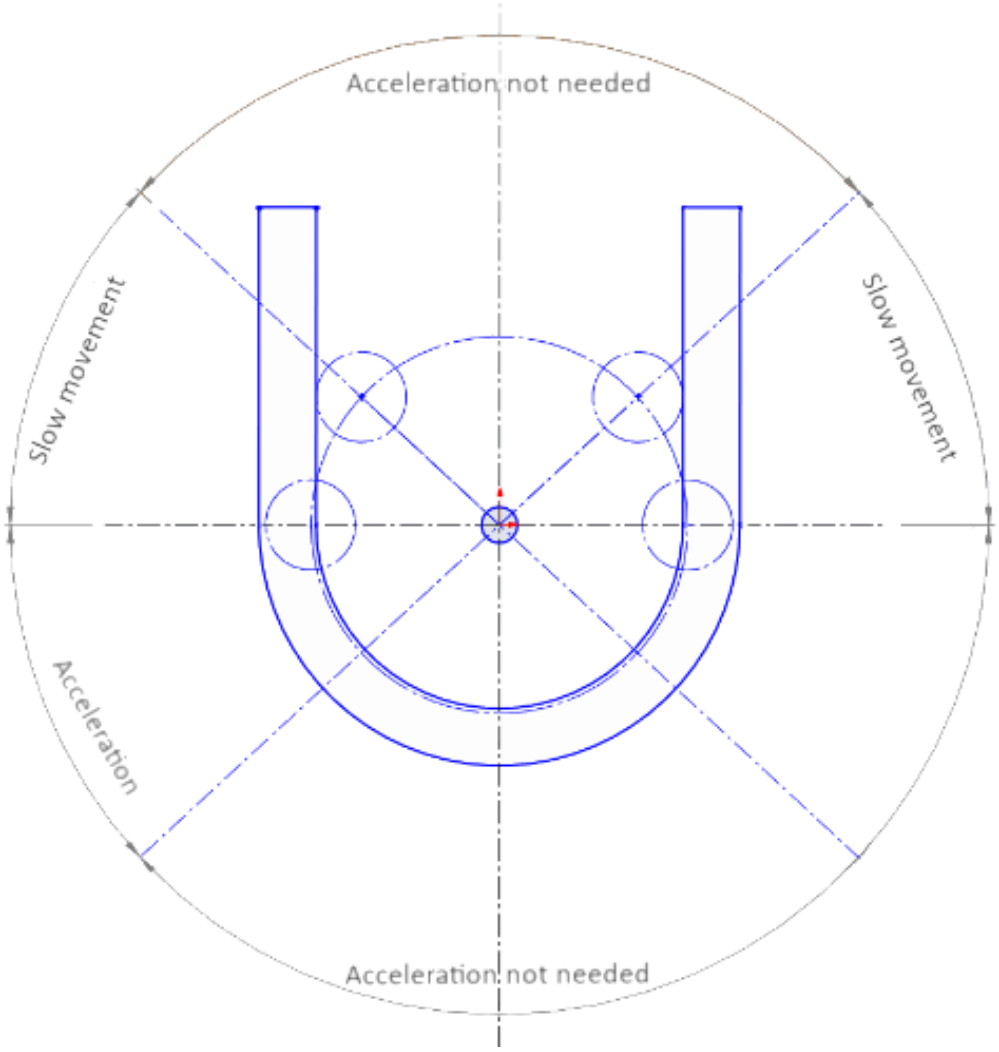

Figure 13 – 180° concept of peristaltic pump

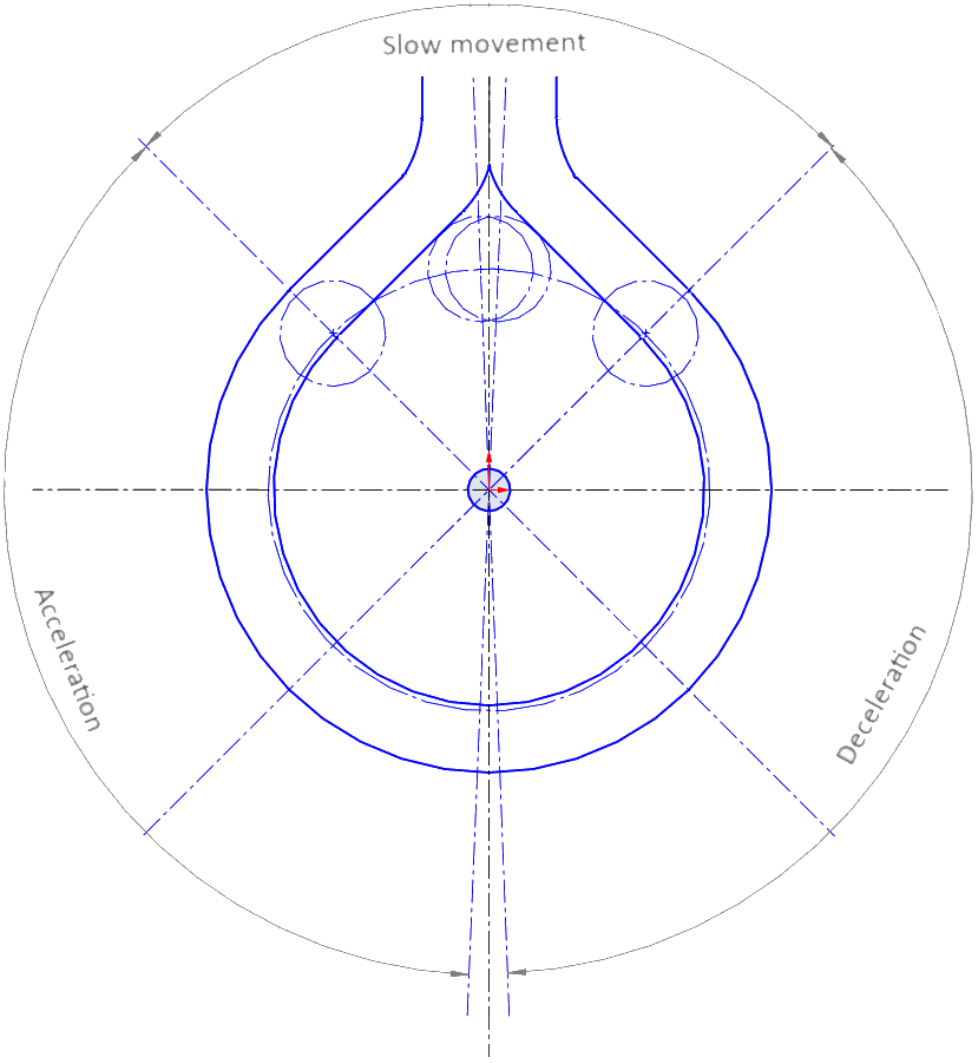

Figure 14 – 270° concept of peristaltic pump

5. Design of peristaltic pump

The following chapter is devoted to the development of suitable peristaltic blood pump for hemodialysis. The peristaltic pump has to cover all the pressure losses in extracorporeal circuit and maintain pressure without high pressure pulses and high shear values, especially during the compression and decompression of the tygon tube. Based on the analytical derivation of the peristaltic movement and numerical simulation, two designs of the pump were created. The first design is based on basic 270° concept from chapter 4 without acceleration of the rollers while the second design aims to increase the pressure in the volume between rollers by changing the acceleration of the rollers to decrease the pressure pulsations during the decompression of the tube.

5.1 Required parameters of the fluid

The blood pump is typically capable to deliver blood at flow rate from 0 to 600 ml/min and is typically set between 300 and 550 ml/min depending mostly on the physiological property of the patient. [15] The flowrate is calculated from the number of revolutions per minute and the volume of tubing segment in the pump. In some machines this value is corrected due to negative arterial pressure (relative to atmospheric pressure), which results in compression and flattening of the tube a therefore in decrease of volume of the tubing segment. For the purpose of the thesis the flow rate during hemodialysis was set to 350 ml/min.

As mentioned before, the arterial pressure before the blood pump is a negative value in relation to atmospheric pressure. The pressure before the blood pump ranges between -80 and -100 mmHg (which corresponds with -13332 Pa) [13] [14]. The pressure is then monitored after it flows through the dialyzer, right before it exits the extracorporeal circuit. The value of venous pressure is around +80 mmHg (+10665 Pa) [13] [14]. The pressure right after the blood pump is usually not measured as it does not provide significant advantages [29]. In order to obtain the pressure on the pressure side of the pump it is necessary to predict the losses in the circuit. Minor (local) losses most notably include losses in arterial and venous access (already accounted for) and pressure loss in dialyzer which can vary with each dialyzer. The pressure drop in the dialyzer was set to 125 mmHg (16665 Pa) [29]. Major losses (due to friction in the tube) are dependent on the length and material of the tubing, which can greatly differ with each hemodialysis unit. In comparison with the local losses major losses are deemed negligible. The pressure profile within the extracorporeal circuit can be seen in Figure 15. The pressure right after the pump can be calculated as follows:

$$p_2 = p_3 + p_{dialyzer} = 27331 \text{ Pa}. \tag{29}$$

The pressure difference of the blood pump:

$$\Delta p = p_2 - p_1 = 40663 \text{ Pa}, \tag{30}$$

where p_1 is pressure before the pump, p_2 is pressure after the pump, $p_{dialyzer}$ is pressure drop in the dialyzer, p_3 is pressure before the blood exits the circuit and Δp is the pressure difference provided by the blood pump.

Typical peristaltic pump efficiencies are near 50 %, but typical peristaltic pumps have flow rate much higher than 350 ml/min. Peristaltic pumps used in ventricular assist device measure efficiency around 34 %. [6]. These measurements were also done for higher flow rates than required so the efficiency will most likely be even lower. For the initial calculation the efficiency is estimated to be around 30 % [6].

Input parameters:

- flow rate $Q = 350$ ml/min
- suction side of the pump $p_1 = -13332$ Pa
- pressure side of the pump $p_2 = 27331$ Pa
- estimated efficiency $\eta_{est} = 30$ %
- blood density $\rho = 1050$ kg/m^3
- blood kinetic viscosity $\mu = 2{,}65$ mm^2/s

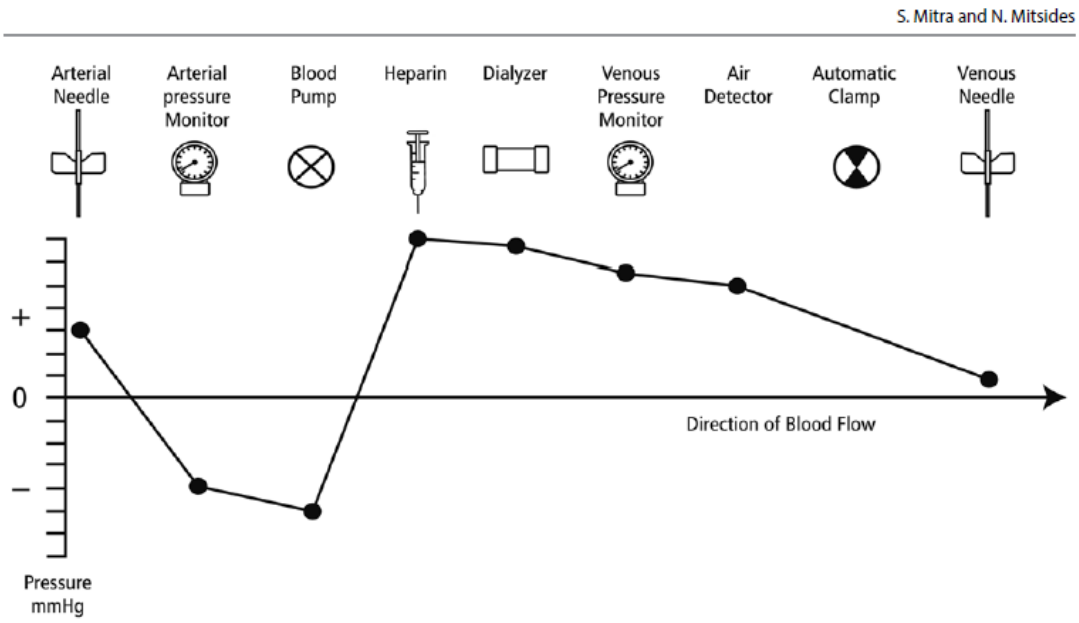

Figure 15 – Pressure profile within the extracorporeal circuit [15]

5.2 Estimation of the power source

One of the most important parts of the pump is the power source. It would be ideal to determine the exact parameters after getting a better idea of the design of the pump through analytical and numerical calculation. But considering the long delivery time, it is necessary to do a rough estimation before any other step to asses if it is possible to use some of the engines already in possession of Department of Fluid Engineering at Brno University of Technology. This means

that the final engine used to power the peristaltic pump can be fairly different from the estimated engine and also different from the ideal one because the parameters can change based on the later calculations.

The main parameters of the pump required to determine the power source are revolutions per minute (rpm), torque and power output. The total power output of the engine consists of hydraulic power and power needed for deformation of the tygon tube. The calculation of both components was done for estimated parameters of the pump – the size of the pump (100 – 180 mm), the size of the roller (20 – 30 mm), the size of the tygon tube (inner diameter 10 – 20 mm). The estimation was done for the basic 180° concept (Figure 13).

The first parameter is the revolution per minute of the pump. This parameter can be determined from the following equation [17]:

$$Q_{th} = V \cdot n \cdot N_{roller} \tag{31}$$

where Q_{th} is theoretical flow rate, V is the volume between the rollers, n is revolutions per minute and N_{roller} is the number of rollers on the rotor. The required flow rate for hemodialysis is around 350 ml/min, the number of rollers 2 and volume can be determined from the inner diameter of the tube and the distance between two rollers alongside the movement of the rollers. The rpm can be now determined as follows:

$$n = \frac{Q_{th}}{\left(\pi \frac{R+r}{2} - d_{roller}\right) \cdot \left(\frac{\pi d_{tube}^2}{4}\right) \cdot N_{roller}} \tag{32}$$

where the first bracket of denominator represents the distance between the two rollers and the second bracket represents the inner cross section of the tube. The results for the different estimated designs range from 2,37 to 4,1 rev/min.

5.2.1 Hydraulic power output

Estimation of hydraulic component of the power output can be easily determined from the required parameters of flow rate and pressure head. The pressure on the suction side of the pump is usually around -100 mmHg (-13332 Pa) and around +205 mmHg on the pressure side (+27331 Pa). As stated in the last chapter the flow rate is around 350 ml/min.

$$\Delta Y = \frac{p_2 - p_1}{\rho} = \frac{27331 - (-13332)}{1050} = 38{,}73 \ \frac{\mathrm{J}}{\mathrm{kg}} \tag{33}$$

$$P_h = \frac{Q \Delta Y \rho}{\eta_{est}} = \frac{\frac{350}{60 \cdot 10^6} \cdot 38{,}73 \cdot 1050}{0{,}3} = 0{,}79 \ \mathrm{W} \tag{34}$$

5.2.2 Deformation of tygon tube

Unlike determination of hydraulic power component, the power required for deformation of the tygon tube is rather complex. The tygon material belongs to the hyperelastic group of materials

which are characterized by hyperelastic deformability and exhibit a stress-strain curve in tension that is non-linear. Therefore, the Hooke's law cannot be used, and Young's modulus cannot be assigned with definitive value except in the region of small strains. Hyperelastic response of rubber-like materials (including tygon) can be best described by constitutive models of hyperelasticity. Even though several constitutive models have been developed over the years, the most widely used is the neo-Hookean model due to its simplicity as it has only one independent material constant [30].

The neo-Hookean constitutive model can be described as:

$$W = \frac{1}{2}G(\lambda_1^2 + \lambda_2^2 + \lambda_3^2 - 3) = \frac{1}{2}G(I_1 - 3) \tag{35}$$

where G can be expressed as:

$$G = NkT;\ G = \frac{E}{2(1+\mu)}. \tag{36)(37}$$

The W is the energy stored in the tygon tube; G is the linear elastic modulus; $\lambda_1\ \lambda_2, \lambda_3$ are the principal stretch ratios; N is the number of chains of molecules per unit volume; k is Boltzmann's constant; T is the absolute temperature; I_1 is the first principal strain invariant; E is Young's modulus and μ is Poisson's ratio.

The linear elastic modulus and Young's modulus for tygon were experimentally determined by the Department of Mechanics and Biomechanics at Brno University of Technology ($E = 1{,}3$ MPa, $G = 4$ MPa) [31]. Unfortunately, because the compression of the tube is not symmetrical, the principal strain invariant I_1 cannot be analytically determined even for a small deformation. Thus, to determine the power required for the tube compression the value must be obtained either by experiment or by numerical calculation using finite element method (software Ansys Structural) [32]. Considering the experiment would require additional resources and would likely be time-consuming we opt for numerical calculation. Even though the experiment would probably be more precise, the less precise values of numerical calculation should be sufficient enough considering we are doing the first rough estimation and the final design of the pump could be fairly different.

5.2.3 Numerical simulation

The simulation was done in Ansys Structural to see how the tygon tube reacts to the compression. For the purpose of simulation three solid models were created – the tube, the roller and the slab which represents the casing of the pump. During the simulation the roller compressed the tube in 1 s to the point where the distance between the roller and the slab was equal to the thickness of the tube. The most important quantity measured was the force required for the compression. The force reaction probe which measured the force in direction z (direction perpendicular to the tube and slab) was set on the roller and on the slab. The material parameters of the tube were defined by Young's modulus and Poisson's ratio determined by the Department

of Mechanics and Biomechanics at Brno University of Technology. The value of Poisson's ratio was calculated by the equation (36)(37).

To calculate the problem as quickly as possible and in the limits of student license, the number of elements/nodes was set to be lower than 32 000. The most refined mesh was used for the tube because the other two solid parts were set to rigid body and therefore do not demonstrate any deformation. The mesh can be seen in Figure 16.

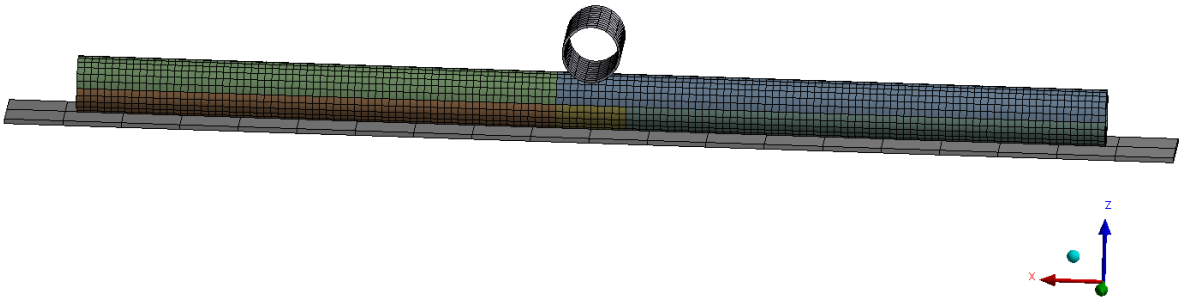

Figure 16 – Deformation of tygon tube (Mesh)

The simulation was completed for different sizes of the roller (20, 25, 30 mm) and different inner diameters of the tube (15, 20 mm). The thickness of the tube was the same for all combinations (2 mm). The results obtained from Ansys Structural can be seen in Figure 17.

Variant	F_d [N]	M_{kd} [Nm]	P_d [W]
D15R30	49,63	3,995	1,742
D15R25	48,68	3,918	1,691
D15R20	38,66	3,112	1,329
D20R30	42,0	3,276	0,83
D20R25	41,8	3,260	0,818
D20R20	41,0	3,198	0,794

Figure 17 - Results of numerical calculation.

To obtain the values of torque and power required for compression it is assumed that the entire force contributes to the torque (is tangential to the movement of the roller). The power output can be obtained from the value of the torque by multiplying the torque by the velocity of the roller given from rpm of the pump (equations (38)(39)).

$$M_{kd} = F \cdot l_{R-r}$$
$$P_d = Mk \cdot \omega \qquad (38)(39)$$

In the equations above Mk_d is torque, F force obtained from Ansys, L_{R-r} the distance between the center of rotation and center the tygon tube, P_d is power and ω is angular velocity of the pump. All the variants are calculated with the same outer diameter of the tube equal to 18 mm.

In reality not the entire force contributes to the torque as only a small component of the force is tangential to the movement of the roller so the power requirement will be lower in reality.

But with this assumption, we can be sure that the parameters of the power output will be enough even if the design of the pump changes after analytical and CFD calculations.

It is worth noting that the proper description of the deformation of the tygon tube is very complicated and an entire thesis could be written on this subject. As can be seen in this chapter, in order to get at least some value of estimated torque and power output, a lot of simplifications and assumptions had to be made. Thus, we can assume that torque, which will be experimentally measured on the final design of the pump, can be vastly different. A more precise characterization of the deformation could be one of the directions for future research.

The total power output can be determined from the hydraulic component and deformation component as follows:

$$P_c = P_h + P_d \tag{40}$$

and from the total power output we get the total torque:

$$Mk_c = \frac{P_c}{\omega}. \tag{41}$$

The total value of power output ranges from 1,58 to 2,53 W and total torque ranges from 4,95 to 6,43 Nm.

5.3 Design

After complete estimation of the power output for the pump, it is possible to finally design two concepts based on the analytical calculations and numerical simulation. Besides meeting the input parameters determined in chapter 5.1 the design of peristaltic pump needs to follow some main principles:

- easily exchangeable and adjustable parts to create pump with different parameters
- low complexity of the design
- reasonable size of the pump
- reduction of friction
- reduction of shifting of the tube
- easy access
- low cost

Considering the pump is mainly intended for research purposes, one of the most important requirements is to be able to swap different parts to adjust the pump for different setups. By doing so it is possible to use manufactured pump for future research – for example it is possible to research the impact of different diameters of rollers, diameters of the tube, different number of rollers, etc. Similarly to this, it is also important to make the design as simple as possible in order to make it less difficult to reassemble, manufacture and access. The simple access is especially important for hemodialysis machine as the tube is usually replaced with each patient. The simplicity of the design also makes the pump cheaper.

The design also needs to minimize the friction between the rollers and the tube as high friction can lead to shorter lifespan of the tube and higher torque on the shaft. The last requirement is to minimize shifting of the tube. The rotation arm can cause the tube to move and shift if not properly supported which can result in asymmetrical stress on the pump. Even though the size is not the main parameter, the pump still has to have reasonable size that could be used in hemodialysis unit.

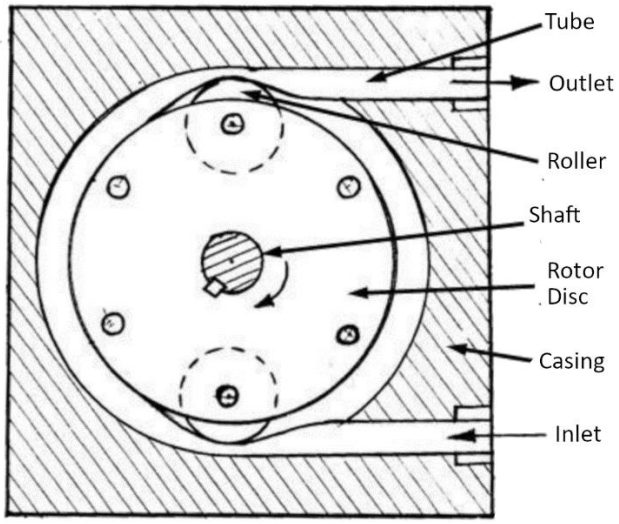

Figure 18 – Simplified schematic of rotary peristaltic pump with rotor discs [17] (edited)

Taking all these principles into account, the rotary peristaltic pump with rollers mounted to rotor discs comes out as the best option (see Figure 18). The rollers instead of shoes reduce friction as they rotate over the tube and therefore do not require additional lubricant to reduce friction. The disc bearing for the rollers comes with an easy option of reassembly and enables to change various parameters related to rollers. Parameters such as number of rollers, diameter of the rollers and occlusion gap can be easily adjusted for future research. This concept also functions with different diameter of the tube and enables an easy access and therefore easy replacement of the tube. Furthermore, the supports for the tube can be mounted to the discs of the rotor and reduce the shifting of the tube.

The low complexity of this option means uncomplicated manufacturing as the only part with complicated geometry is the casing. This results in lower cost of the design because not all the parts have to be created on 3D printer. The design can also be quickly adjusted provided that the pump will not work optimally.

5.3.1 First design – basic concept

As stated before, the first design is based on the "270° concept" from chapter 4 where the roller travels 270° in a fully compressed state. Because the first stage of numerical simulation did not provide reliable information (see Chapter 6.4) to justify buying specific tygon tube, it was decided to use the tube already in the possession of Department of Fluid Engineering at Brno

University of Technology. The important parameters of tygon tube can be seen in the list of input parameters. Considering the tube is replaced during hemodialysis with every patient the occlusion was set to 20 % (fixed in the entirety of the pump).

The diameter of the casing holding the tube was established to provide smooth deformation of the tube on inlet and outlet. It is anticipated that the slower the trajectory of the tube deviates from the trajectory of the roller, the smoother is the reflux on the outlet and pressure hammer on the inlet because the deformation of the tube is less sudden. The diameter was set to 160 mm because for lower values the angle of deviation of trajectories was assumed to be too high.

The higher number of rollers can lower the amplitude and increase the frequency of pressure pulses and lower the volume of fluid transported with each revolution. Even though this impact makes the number of rollers an important parameter of the design it is not part of the thesis as proper determination of the impact of the rollers would be too time consuming. Therefore, determination of the impact of the number of rollers could be subject of future research. Similar argument can be applied to the support rollers. The number of both rollers and support rollers was set to 2 with diameter of 30 mm.

Input parameters of the pump are:

- diameter of the casing: $D = 160$ mm
- diameter of the roller/support roller: $d_{roller} = 30$ mm
- number of rollers: $N_{roller} = 2$
- number of support rollers: $N_{sup} = 2$
- tygon tube:
  - inner diameter of the tube: $d_{tube} = 13$ mm
  - thickness of the tube wall: $t = 1{,}5$ mm
  - occlusion: $O_c = 0{,}2$ (20 % − fixed)

For briefness only the most important calculation will be shown in the main part of the thesis. The MS excel file containing rest of the calculations can be seen in the appendix.

The occlusion gap between the roller and the casing:

$$s = 2t(1 - O_c) = 2{,}4 \text{ mm} \tag{42}$$

The outer diameter of the tube:

$$D_{tube} = 2t + d_{tube} = 16 \text{ mm} \tag{43}$$

The distance between the center of rotation and center of the roller:

$$R_r = \frac{D}{2} - \frac{D_{roller}}{2} - s = 62{,}5 \text{ mm} \tag{44}$$

The distance between the center of rotation and center of the support roller:

$$R_{sup} = \frac{D}{2} - \frac{D_{tube}}{2} - \frac{D_{roller}}{2} = 57 \text{ mm} \tag{45}$$

The cross section of the tube:

$$S_{tube} = \frac{\pi {d_{tube}}^2}{4} = 132{,}7 \text{ mm}^2 \tag{46}$$

The length between rollers:

$$l_{180} = \pi \left(\frac{\frac{D}{2} + \left(\frac{D}{2} - D_{tube}\right)}{2} \right) - \frac{D_{roller}}{2} = 226{,}2 \text{ mm} \tag{47}$$

The volume between rollers:

$$V_g = S_{tube} L_{180} = 2{,}8 \cdot 10^{-5} \text{m}^3 \tag{48}$$

The rpm (respectively rps) of the pump can be determined using equation 32 from chapter 5.2:

$$n = \frac{Q_{th}}{V_g N_{roller}} = 0{,}104 \; s^{-1} = 6{,}24 \text{ min}^{-1} \tag{32}$$

Based on the main dimensions of the pump it is now possible to design all the parts of the pump (the dismantled peristaltic pump can be seen in Figure 19):

- casing
- 2 rotor discs
- 2 rollers
- 2 support rollers
- shaft
- housing of the bearings
- the lid of the housing
- 2 bearings

The thickness of the casing wall supporting the tube is 10 mm as its purpose is to sustain the load affecting the tube. The thickness of the remaining walls is 6 mm. The area of inlet and outlet is provided with a "nose" to further support the tube and provide guidance in exiting the casing. The "nose" is cut in shape of the tube to provide better fit. A significant part of the back wall was cut out to save material in printing. Even though it would have been better if the casing and the housing of the bearings were in one part, it was decided to print the parts separately and then screw them together as it requires less supporting material during the printing. The bottom section of the pump was provided with supports. In practice the pump is implemented to

hemodialysis unit and does not need any additional support but for the purpose of experiment the supports had to be provided.

The thickness of rotary discs is 3 mm. The discs can be preadjusted with series of holes in the radial direction as well as peripheral direction to ensure the possibility of variable configuration of rollers and roller supports. The holes for the roller and roller supports are drilled with the same diameter to allow interchangeability between the position of said parts. Four holes in the middle of the discs were drilled to allow the assembly with the shaft.

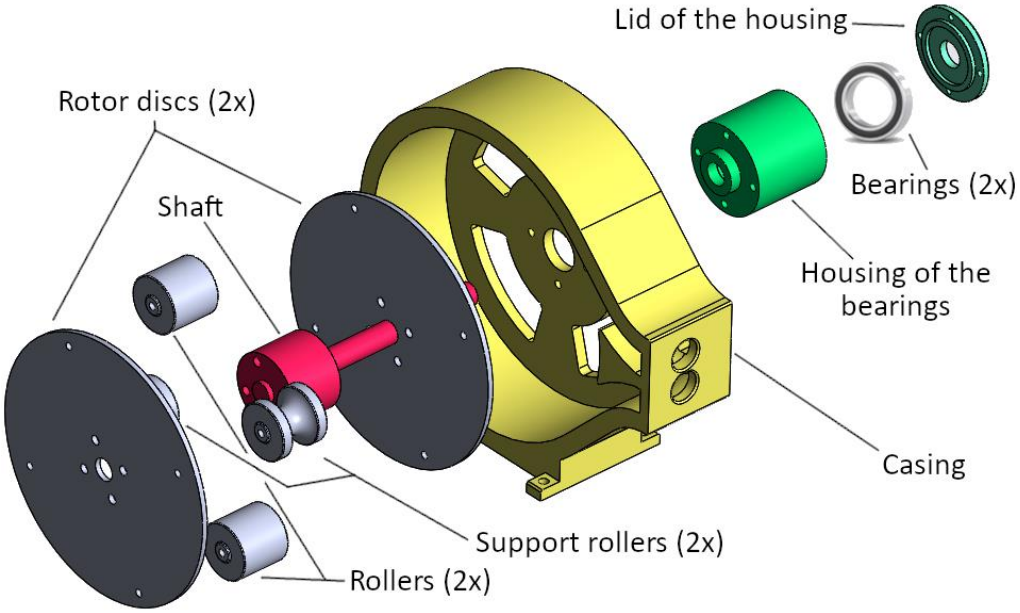

Figure 19 – Dismantled design of peristaltic pump

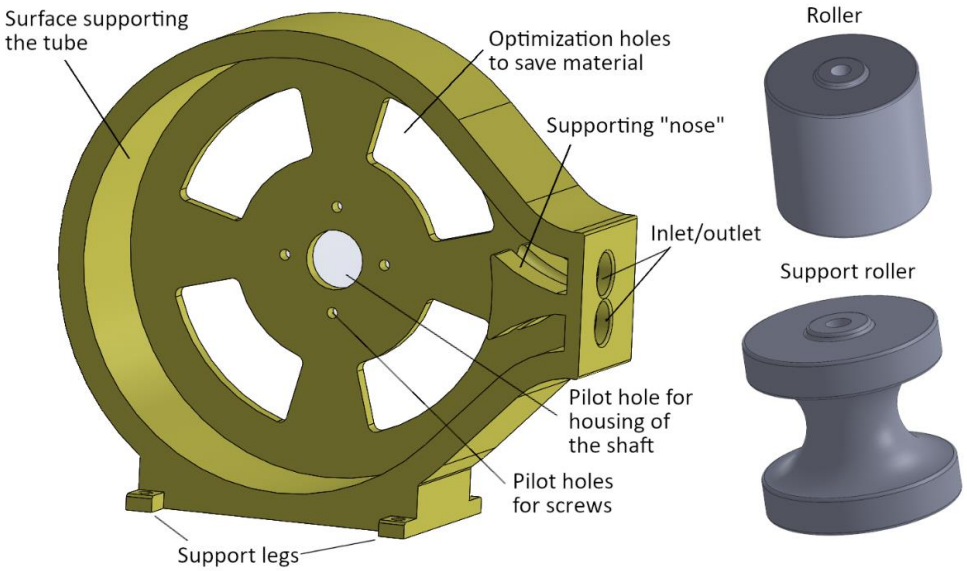

Figure 20 –Casing (left), support roller (bottom right), roller (top right)

The rollers and the roller supports have to be the same height, otherwise it would not be possible to assemble them together. The height has to be higher than the width of the tube in the most deformed state to ensure the tube does not compress around the rollers. The width was established at 24 mm and therefore the height of the rollers was set to 30 mm to provide a reserve considering the possible shifting of the tube. In the final design of the pump each roller has its own bearings to provide rotation with the least possible friction, but for the experimental purposes the rotation is possible due to internal looseness between the rollers and the disk. Lubricant is applied to further improve sliding property.

The rotation of the main shaft is ensured by providing housing with two 16101 2RS ball bearings. As mentioned before, the housing had to be screwed together with the casing to lower the cost of supporting material during the 3D printing. The axial movement of the shaft is prevented by two retaining rings. The bearings are designed in a way in which the second bearing and the line of action of the force affecting the rotor are in the same distance from the first bearing. The symmetrical setup should reduce excessive shaft deflection during the operation of the pump. The shaft is most prone to deflection when only one roller is compressing. If both rollers are maintaining constant movement the shaft's deflection is lower because the rollers support each other, therefore the force affecting the rotor is reduced. The layout of the bearings and shaft can be seen in Figure 21.

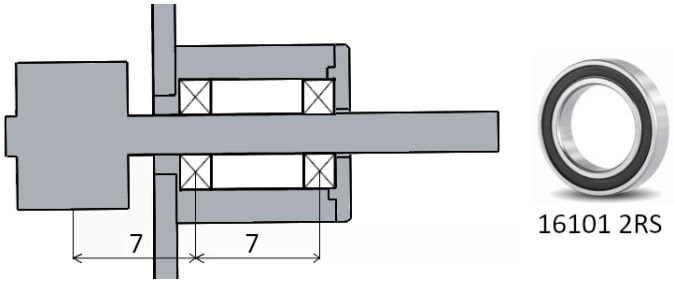

Figure 21 – Layout of the bearings and shaft

Considering blood does not come into contact with any part of the pump except for the tygon tube, it is not necessary to pay increased attention to the compatibility of the materials with blood. Therefore, it is possible to use standard ABS (acrylonitrile butadiene styrene) material for the parts printed in the 3D printer (the casing, the support rollers, the housing of the bearing and the lid for the housing). Steel was used for the shaft and rest of the parts were created from plastic materials.

5.3.1 Second design – elliptic concept

The second concept comes from the basic design but uses variable diameter of the supporting casing to achieve acceleration of the roller during fully compressed peristaltic movement which can possibly result in increased pressure in the volume between rollers. As stated in chapter 4.3.2, the decreased pressure difference in front of and behind the leading roller should result in lower amplitude of the pressure pulse during the reflux. While the adjustment of the casing

is relatively simple (changing circular design of the casing to elliptical), the adjustments of the roller supports are rather complicated. It is not possible to use the two discs concept because the distance between the center of the roller and the center of the rotation has to change to ensure the same level of occlusion during the entirety of the peristaltic pump movement. Schematic of possible design can be seen in Figure 22.

A roller mounted to a sliding extendable arm could solve this problem. The extendibility would be provided by loaded mechanical or pneumatic springs. The usage of springs is common among the manufactured medical peristaltic pumps, but they are used to ensure the same level of occlusion for different diameters of tubing and to make the compression and decompression smoother. Utilization of springs to accelerate rollers does not appear among frequently used medical peristaltic pumps. The force required to keep the exact occlusion during all stages of the pumping could be determined by numerical simulation, but a better approach is to use values obtained by an experiment carried out with the basic design from previous chapter.

The usage of extendable arm comes with an obstacle – how to attach the arm to the carrier mounted to the rotor. A possible design can be seen in Figure 22 and Figure 23 where the attachment is solved by a telescopic tube which would extend from the carrier, also in the form of tube. The carrier would have to be adjusted with leading grooves to prevent shifting of the extendable arm due to the contact with tygon tubing. The carrier and extendable arm would have to be from a material that allows sliding without high friction (for example Teflon) and lubricant would have to be applied to the surface to decrease the friction even more.

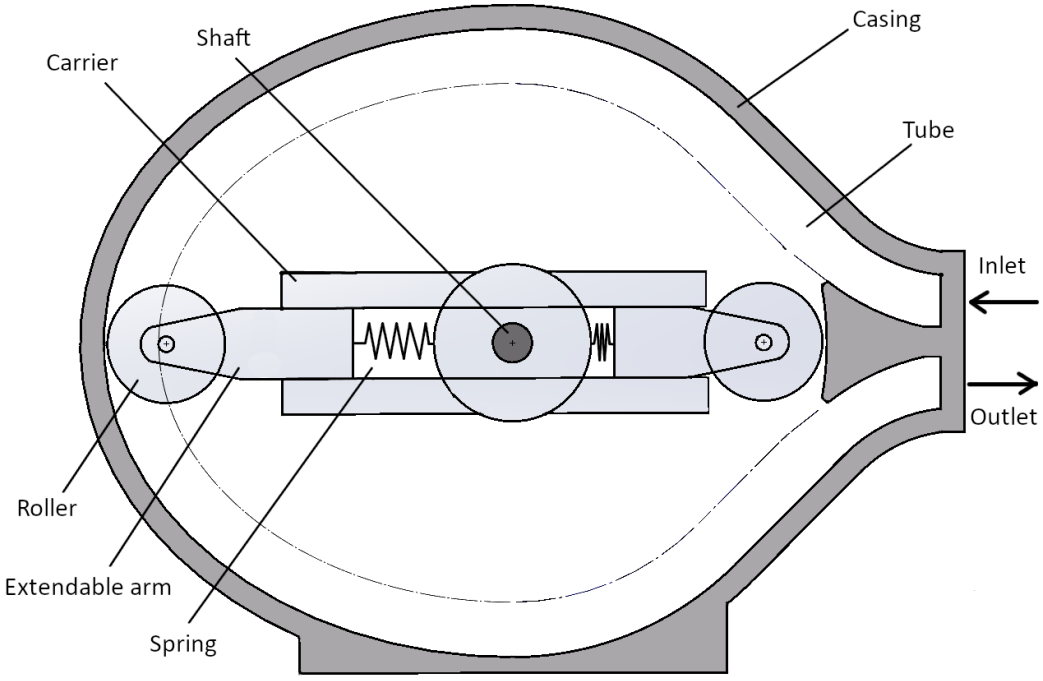

Figure 22 – Schematic of elliptic peristaltic pump

Unfortunately, the design with variable acceleration was not finished, especially due to difficulties with numerical simulation which took more time than previously estimated, and therefore is a subject for future research. Considering the second design will probably not be as easily adjustable as the first design, the most prominent approach would be to acquire enough data from experimental research of the first design and use this information to finalize the second design. It is necessary to determine the force required for the springs as well as define the optimal number of rollers, optimal diameter of the tygon tube and the influence of the support rollers on the shifting of the tube. With this information it is then necessary to design proper way of attachment of the carrier to the rotor.

The casing can be improved as well. The trajectory possible for acceleration (see Figure 14 from chapter 4.3.2) starts sooner and ends later than in the current design where only half of the pump is in the elliptic shape. The casing would also have to be optimized to provide smooth transition of the roller from outlet to inlet. Furthermore, it would be interesting to research whether the casing could be adjusted in such way that the springs would not be required. If the sum of distances between the rollers and center of rotation was the same through the whole movement, it would be possible to design an extendable arm connecting the rollers at a fixed distance. The extendable arm could then slide in one way or the other based on the shape of the casing while keeping the occlusion gap constant. This solution is elegant as all issues connected to the springs would disappear, but it is not apparent whether the casing could be shaped in such a way and whether it would not be unfavorable to the overall design.

It is also worth mentioning the possibility of using pneumatic springs instead of mechanical ones. Pneumatic springs would come with the obstacle in the form of leaking, but it may turn out to be more elegant design.

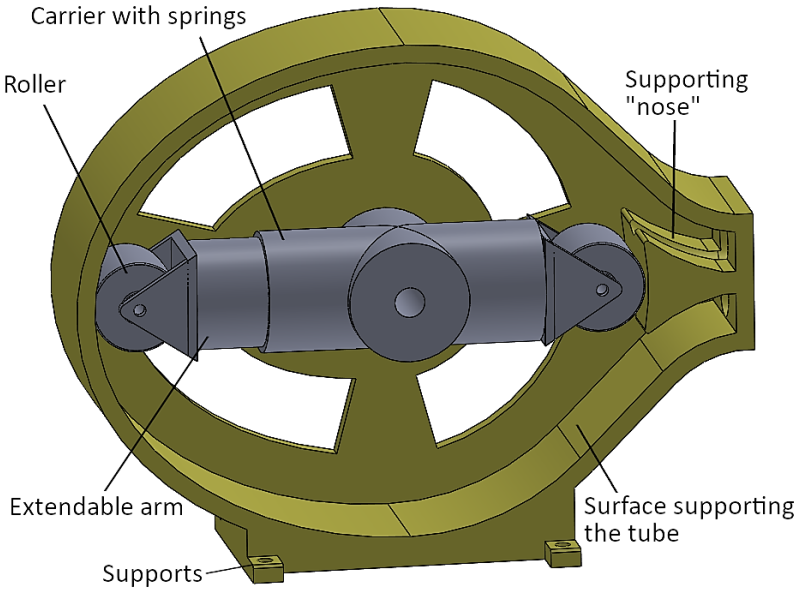

Figure 23 – First design of elliptic peristaltic pump

6. Numerical simulations

The following chapter is dedicated to numerical simulation of the flow inside the tube during the movement of peristaltic pump calculated in Ansys Fluent. The objective is to create a 2D model that will be able to simulate pressure pulses during the compression and decompression of the tube. Simulation is invaluable because it provides helpful information about the impact of various parameters of the pump on the final character of the flow without the need to manufacture high number of components for experimental research, thus saving money and time. It can also provide better perception of the flow inside the pump which endorses new ideas and can result in better designs.

The creation of a numerical model can be dived into 3 phases. In the first phase simulations were done for different configurations of geometry parameters and the main goal was to adjust the model to calculate as physically accurate results as possible. In other words, to create a model that would estimate the dependency of pressure pulses on various factors of the design. In the second phase the model was adjusted to correspond with the first design of peristaltic pump (see Chapter 5.3.1). In the third phase the model was expanded on by the possibility to adjust acceleration to correspond with the second design which has elliptic shape of the casing.

6.1 Simplifications of simulations

Considering the design of the pump is not based on any previous research carried out by Department of Fluid Engineering, one of the main objectives is to lay fundaments for future research. Therefore, it is beneficial to make the model as simple as possible, so it grants possibility to simulate as many different parameters of the pump as possible.

Hence it was decided to make the model in 2D because it demands the lowest requirements for the complexity of scripting defining the peristaltic movement and the lowest demands on computational power and time. Even though the 2D simulation is the most convenient choice, it is important to point out that 2D simulation is not the most satisfactory choice for simulation of vortices appearing during the reflux as vortices cannot emerge and dissolve in 2D. Simulation of vortices in Ansys Fluent in therefore not as accurate in 2D as it is in 3D. Equation (49) represents production component of vorticity equation [33]. We can see that, for 2D flow, the production component equals zero.

$$\omega_1 = \omega_2 = 0; v_3 = 0 \rightarrow \omega_j \frac{\partial v_i}{\partial x_j} = 0 \tag{49}$$

The other option is to perform the simulations in 3D which results in a more accurate outcome but the scripting behind the peristaltic movement is too complex and the number of elements would rise enormously. Therefore, it is better to perform 3D calculation of finalized pump design where the simulation can be validated by experiment. Also, it is beneficial to execute the simulation as Fluid Structure Interaction (FSI) of the whole pump which combines the structural analysis from Ansys Structural with flow analysis from Ansys Fluent. It is the most precise method, but it is also the most complex as it is necessary to have good understanding of

mechanics and hydromechanics behind the simulation. Using FSI it is also possible to model the effect of pressure pulses on the deformation of the tube. Furthermore, it is a better option when it comes to complexity of scripting as the movement is conveniently defined in Ansys Structural and therefore the deformation of the wall does not have to be prescribed by user defined functions (UDF) in Ansys Fluent.

Similarly to the analytical analysis, the curvature of the tube is disregarded and therefore considered to be linear. This simplification is especially helpful for scripting of the peristaltic movement as linear movement is easier to prescribe than rotational movement. Also, the fluid is defined as incompressible and gravitation is negligible.

Even though the blood pump is supposed to transport human blood, water was set as a fluid for the simulation. Considering water will be used for the experiment, it is better to perform the simulation with the same fluid to ensure that input conditions are as close as possible. The density of water was set to 998,2 kgm^{-3} and dynamic viscosity to 0,001003 $kgm^{-1}s^{-1}$. Water is commonly used in experiments as it closely resembles blood and therefore the differences will be insignificant.

Summary of simplifications made:

- 2D simulation
- disregarded curvature of the tube
- incompressible fluid
- disregarded gravitation
- water instead of blood
- compressed shape prescribed by regressed function (see Chapter 6.3)
- Adjusted occlusion gap

6.2 Simulation settings

6.2.1 Solver

A pressure based absolute transient solver was used for the simulations. The model was set as realizable k-ε with non-equilibrium wall function. The k-ε model is a two equations model that comes from the closure problem of Reynolds averaged Navier-Stokes (RANS) equations which are used for simulation of turbulent flow. The realizable variant of k-ε model is newer and provides more accurate results by taking a different approach in defining the turbulent viscosity. The non-equilibrium wall function describes the flow in boundary layer near the walls. By applying wall function to the solver, it is possible to use coarser mesh which results in lower demands on computational power. The methods of the solver were first set to standard or first order upwind and after convergence changed to the second order upwind for momentum and turbulent equations. The method for pressure equation was set to linear and kept the same through the simulations. The under-relaxation factors were set to default.

6.2.2 Domain

In Figure 24 we can see the starting geometry of the domain as well as state of the domain during the simulation (specifically during the compression by the second roller). This particular geometry was created for tube with inner diameter of 10 mm, roller with diameter of 30 mm and basic 180° concept. In the figure we can see the boundary conditions, zones of the domain and details of significant parts of the mesh.

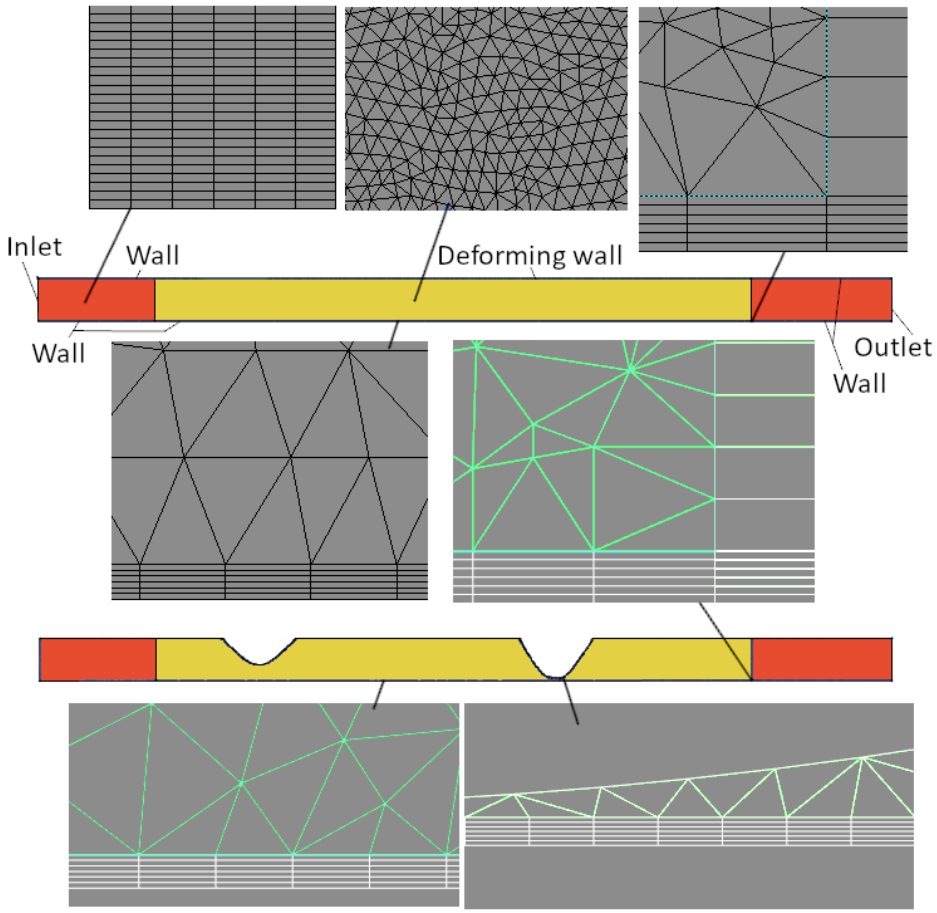

Figure 24 – Mesh and boundary condition of the domain (starting domain - top, domain during compression - bottom)

The starting domain contains three zones – the zone near inlet and outlet composed of quadrilateral cells, the main deforming zone composed of triangle cells and the small zone along the bottom edge composed of quadrilateral cells. The domain is composed of 2 types of cells because in order to simulate flow with deforming wall, it is necessary to use remeshing (more about remeshing in chapter 6.3). Unfortunately, the remeshing functions only in zones with triangle cells so it is impossible to use structured mesh which would decrease the number of elements. The small quadrilateral layer near the bottom wall contains only 6 elements in the direction x_2 and its purpose is to ensure at least 6 cells are located in the area between the bottom wall and fully compressed top wall. If the layer was not present, the remeshing would

assign only one cell into the gap which would not be enough to ensure authentic velocity profile. The mesh in the area between the walls in fully deformed state can be seen in Figure 24.

The number of elements is under 512 000 for the initial state to stay under the limit of student license, but in some cases the number rose above the limit due to enabled remeshing option. The zone with triangle cells is rather large as it needs to represent the entire tube in the peristaltic pump. A large zone, that needs to have unstructured mesh due to remeshing, results in high number of elements which means that the mesh cannot be very refined while staying under the student license. Fortunately, in some cases coarse mesh works better with remeshing because nodes of the moving edge cannot move more than approximately 1 length of the element per 1 timestep, otherwise the negative volume error occurs (see Chapter 6.3.1). This means that for fast movements with refined mesh the size of the timestep has to be very small resulting in high demands on computational time. Additionally, the UDF prescribes the movement for each cell separately (see Chapter 6.3) which means even higher relation between computational time and number of elements. Considering the 2D model is intended for quick initial simulations it was decided to persist in simulating with coarse mesh and leave the optimization for future research.

The boundary condition can be seen in Figure 24. The top wall represents the deforming wall compressed by the roller (see Chapter 6.3) while the rest of the walls were defined as stationary walls. For inlet and outlet two combinations of boundary conditions were used. Because the velocity inlet and pressure outlet option resulted in error in almost all cases, most of the simulations were calculated with pressure inlet and pressure outlet boundary conditions. In the later stages the velocity profile obtained from pressure-pressure simulation was used as a velocity inlet for velocity-pressure simulation. By providing pulsating velocity profile the simulation was less susceptible to errors and it was possible to acquire additional data. More about the subject of boundary condition can be seen in chapter 6.4.

6.3 Wall deformation

The deformation of the wall corresponding to peristaltic pump movement is defined by UDF which was written in programming language C which is used by Ansys to define more complex calculations like defining movement of the wall, movement of the nodes, transient velocity profile, etc.

The deformation of the wall can be divided into three parts – the compression at the beginning of the domain, the constant movement in the x_1 direction and decompression at the end of the domain. The compression and decompression in the direction x_2 means there is relative movement between the nodes and therefore the moving edge cannot be defined as rigid body. Thus, it is necessary to use a function called DEFINE_GRID_MOTION [34] which allows updating the position of each node separately.

DEFINE_GRID_MOTION(name, domain, dt, time, dtime)

The main problem, that arose during the initial attempts, was that the edge representing the roller moved in the direction x_1 to the end of the domain (therefore executing one revolution), but then was unable to skip back to the beginning of the domain because the nodes of the edge cannot travel more than approximately 1 length of the element during 1 timestep. In other words, only one revolution of the pump could be executed which is not enough as the transient calculation stabilizes after a couple of periodical revolutions.

Based on this revelation it became apparent that the movement has to be connected to some entity that is not part of the mesh domain and the deformation has to be carried out by the movement of nodes in direction x_2 which would be prescribed to each node of deformed edge (similar to the wave motion). By doing so the transition from the end to the beginning of the domain would not be a problem. Based on the numerical simulation (from chapter 5.2.3), the estimated shape of the deformed edge was created in Ansys Modeler and the coordinates of the final shape were extracted into text file. The coordinates were then imported into MS Excel where Excel's regression tool was used to obtain a function which corresponds to the waveform of the deformed wall. An example of difference between the coordinates from Ansys and the calculated coordinates can be seen in Figure 25. The function varies for different configurations of tube diameter and roller, but for similar configurations it can be quickly adjusted by changing the absolute value which represents the maximum distance of deformation. This means that the calculation can be quickly adjusted for various gaps between the tube and the roller.

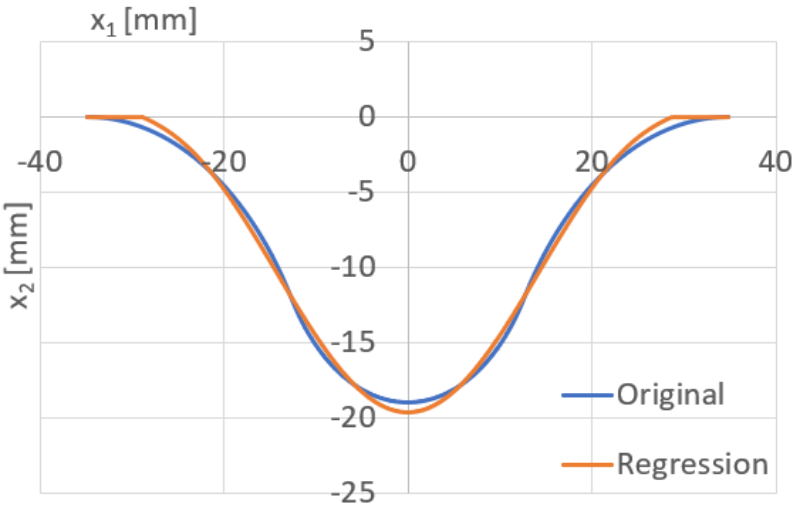

Figure 25 – Difference between values from Ansys Fluent and calculated values

$$x_2 = 4 \cdot 10^7 x_1^6 + 1{,}2979 x_1^5 - 79572 x_1^5 - 0{,}0009 x_1^3 + 56{,}875 x_1^2 + 3 \cdot 10^{-8} x - 0{,}0145 \quad (50)$$

As can be seen in Figure 25, the shape is a function of distance from point [0,0] which can be interpreted as the x_1 position of the center of the roller. By moving this point (C)[3] along the deforming edge it is possible to simulate the deformation without the need to move any real edge (which could result in error during simulation) only by moving the nodes of the edge in the direction x_2. With increasing distance from point C the x_2 coordinates of respective nodes approach 0 and eventually cross the axis into the zone of positive values. The function is completed with condition that any positive values of coordinate x_2 are replaced with 0 to ensure that the shape of non-deformed tube remains the same. Also, if the value of distance between the node and the leading point C is too high and the influence is therefore negligible, the calculation of x_2 coordinate is not performed. By doing so a lot of computational time is saved as the calculation is carried out only for nodes close (in area of influence) to point C.

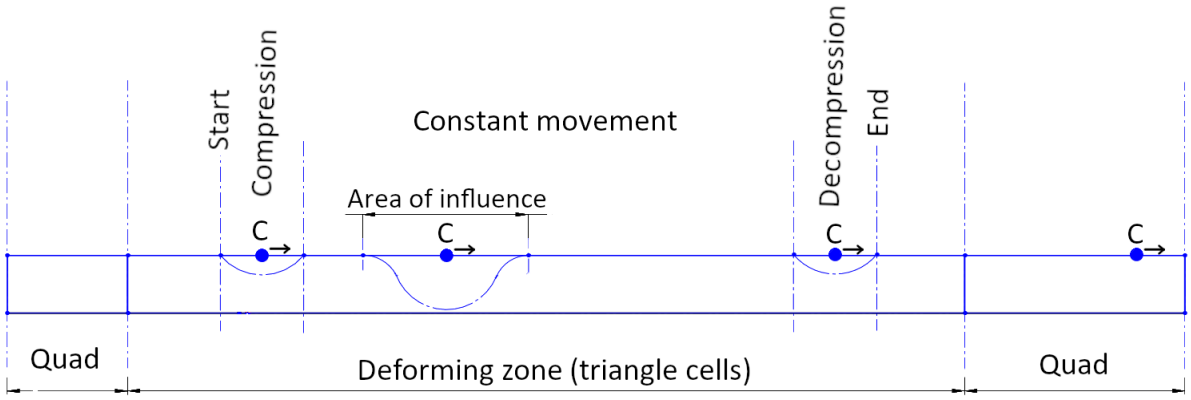

Figure 26 – Stages of peristaltic movement

The previous method solves the constant movement during the fully deformed state. To adjust the script for the compression and decompression, the function is expanded on by including sinus (respectively cosine) as a function of simulation time which provides gradual transition from the non-deformed to the fully deformed state. We can see the stages of movement in Figure 26. The line between the stages is calculated in the script as a function of rps (revolution per second) and the angle of deformation (the angular displacement of the roller during the compression or decompression). Considering control point C exists only in the script and does not have a real form in Ansys Fluent, when it reaches the end of the domain it continues in the same direction until the simulation time is equal to the time of 1 revolution (360°) and then its position changes to the start of the movement. The movement continues in the same way until the calculation is finished. The same function is prescribed to the movement of the second roller only the start is delayed by 180°. The part of the code responsible for the movement can be seen in Figure 27 (the whole script is enclosed in the appendix).

[3] The point which represents the center of the roller is labeled as S in the script. To avoid confusion with deforming surface from chapter 4 which is already called S in the thesis, the center of the roller was relabeled to C in the thesis but remains as S in the script which can be seen in the appendix.

```
/*position of active node (x,y direction)*/
x0 = NODE_X(node_p);
y0 = NODE_Y(node_p);
/*relative position to the leading points*/
x_rel1 = S_roller1 - x0;
x_rel2 = S_roller2 - x0;
/*calculation of new y position for nodes effected by roller 1 */
if (fabs(x_rel1) <= x_max) {      /*Area of influence*/
if (S_roller1 <= distance_def) {  /*Compression*/
y_new1 = geo_function1 * sin( (M_PI/2) * (timer1/time_def));
}
else if (S_roller1 >= (distance_def + time_180 * vel_x) /*Decompression*/
          && S_roller1 <= (2 * distance_def + time_180 * vel_x)) {
y_new1 = geo_function1 * cos( (M_PI/2) * ((timer1-time_def-time_180)/time_def));
}
else if (S_roller1 > (distance_def) /*Constant movement*/
          && S_roller1 < (distance_def + time_180 * vel_x)) {
y_new1 = geo_function1;
}
if (y_new1 > 0) {
y_new1 = 0;
}
NODE_Y(node_p) = y_new1;  /*Transition of new position into cell*/
}
```

Figure 27 – Part of the code responsible for peristaltic movement

The input values for the code are rps, angle of deformation, deformation function for the specific geometry, length between the rollers and area of influence of control points C. Even though some of these values can be calculated via the UDF, the input values are not required to be changed often as usually only the rps is changed between the calculations and therefore the calculations were done in MS Excel and then input into the script. This approach helps with computational time and clarity of the code. The example of calculations in MS Excel can be seen in the appendix. The code can even be quickly adapted for different number of rollers as the function defining the movement is the same and can be copied with adjustment of the length between the rollers. This fact is valuable for future research with more than just two rollers. The complete script is then compiled as UDF in Ansys Fluent and prescribed to the deforming wall in dynamic mesh settings. It is necessary to run the UDF in compiled mode because some functions (including DEFINE_GRID_MOTION) do not work in interpreted mode.

6.3.1 Dynamic mesh settings

As for the dynamic mesh methods, remeshing and smoothing were applied to the zones with triangle mesh. All zones were set as deforming with maximum and minimum length scale equal to the starting values obtained by "zone scale info" function and with maximum skewness

of 0,7. All edges except the deforming edge were set as stationary with cell height based on the starting mesh. The deforming edge were set to user-defined and associated with UDF mentioned in the previous chapter. Both methods, with and without the solution stabilization, were tested (coefficient-based with scale factor 0,3).

Smoothing allows deformation of the mesh near the walls in order to refine the mesh during the grid movement. For the simulation we used spring-based method which, roughly speaking, means that the mesh is deformed in a similar way as the spring would be. The deformation can be controlled by changing the spring stiffness by adjusting the value of Spring Constant Factor which can be set to a number between 0 and 1 [35]. The calculations were tested with various values and it was concluded that 0,5 results into most stable mesh during the movement. The convergence tolerance was set to 0,001 and the number of iterations to 20. The effect of spring-based smoothing can be seen in Figure 28.

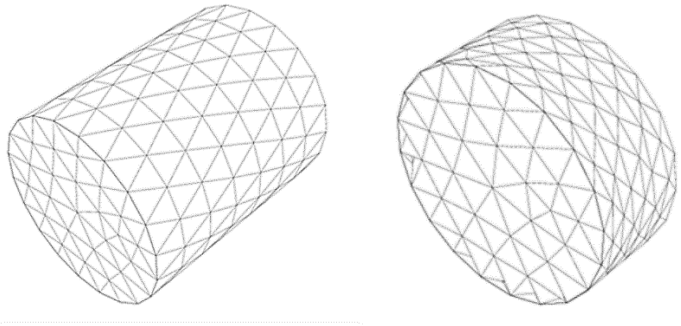

Figure 28 – Spring-based smoothing (before deformation, after deformation) [35]

During the simulation with small deformations typically only smoothing is required, but when the boundary displacement is large in comparison to the cell sizes, the cell quality can deteriorate, resulting in error, for example due to negative mesh cell volume. Remeshing option solves this problem. The cells which do not satisfy the skewness or size criterion are locally updated into new satisfactory mesh [36]. The deformation due to peristaltic movement is large in comparison to cell sizes and therefore remeshing is required. Remeshing method was set to local cell with size criterions set as default (based on starting mesh) and skewness set to 0,7. Size remeshing interval defines the number of timesteps between the remeshing based on the sizing criterion. The cells that exceeds the skewness are remeshed immediately. The variants between 1 and 5 were tested during the calculations. The remeshing interval of 1 is best during the compression and decompression as the mesh is the most susceptible to error. For the rest of the simulation it is convenient to keep the remeshing interval close to the value of 5 as the remeshing is not necessary that often. Ideally, if the simulation is susceptible to error, the remeshing interval can be manually changed to 1 during the decompression and then changed back to 5 during the constant movement. It would be beneficial to investigate whether it is possible to include a variable remeshing interval into the UDF. The sizing function was enabled

which means that the cells are marked based on size distribution[4]. The values of resolution, variation and rate were set to default.

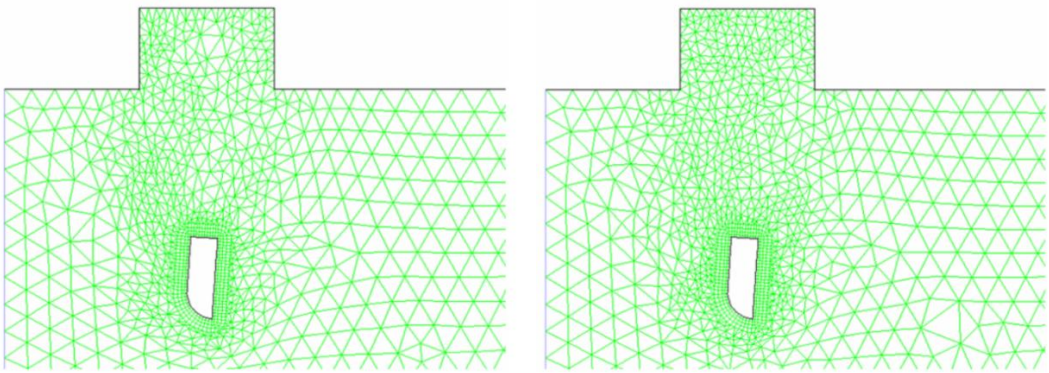

Figure 29 – Remeshing without (left) and with (right) size functions [36]

6.4 The first phase of simulations

The objective of the first phase of simulations was to create a working model that would predict the dependency of pressure pulses on various factors of the design. As most of the time was spent on testing different configurations of the calculation, adjustments to the script and adjustments to the remeshing, only three different geometries were simulated during the first phase. The parameters of the geometries were diameter of the supporting casing and diameter of the tube – specifically variant D100d15, D100d10 and D150d10 (D – diameter of the supporting casing [mm]; d – diameter of the tube [mm]). The simulations were carried out for different values of rps ranging between 0,2 and 0,8 rps (12 and 48 rpm). The values of rps are vastly different from estimated revolutions of the first design because the simulations were carried out before the design was finished and it was anticipated that the design would be smaller. But the information obtained from the simulations with higher rps will likely be valuable even for the design with lower rps. All simulations were performed for the 180° concept.

As mentioned before the first phase was carried out with pressure-pressure boundary condition (27331 Pa on the outlet and -13331 Pa on the inlet, relative to the atmospheric pressure). During the simulation the values of pressure and velocity were monitored. Specifically, pressure and velocity (in the direction x_1) on the inlet/outlet and pressure on the iso-surface in the distance of 0,1 and 0,15 m from the coordinate $[0,0]$ which corresponds to the start of the compression. The pressure course had to be measured on iso-surfaces that were in sufficient distance from inlet and outlet because we assume that constant unrealistic pressure boundary conditions

[4] The rules of sizing function, based on which Ansys Fluent marks the cells, are too long to include into the thesis. However, sizing function is an important part of remeshing function and therefore should not be neglected. For more information, see the Ansys Fluent manual [36].

restrict pressure rises in the system. The pressure course measured on iso-surface ($x = 0{,}1$) as well as pulsating velocity on the inlet and outlet can be seen in Figure 30 and Figure 31.

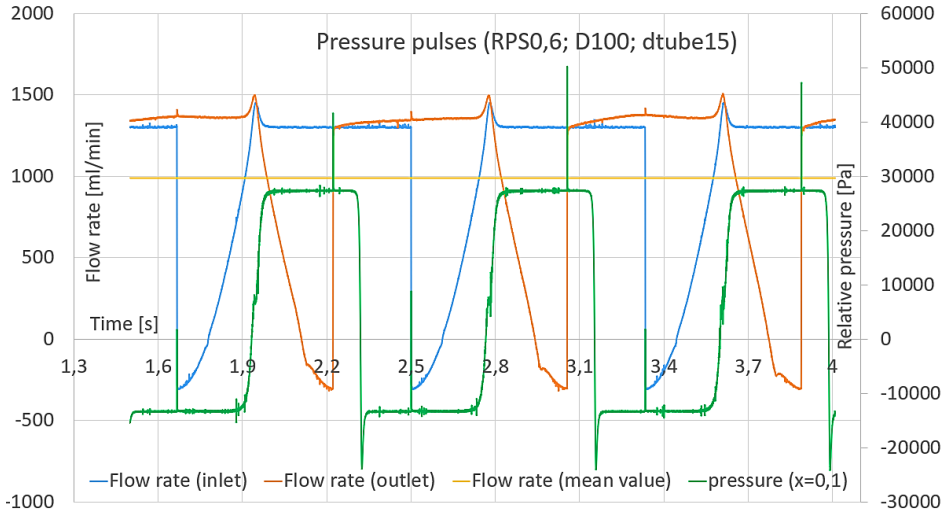

Figure 30 – Pressure pulses and flow rate during compression and decompression

Based on the charts we can confirm that pressure pulses occur both during the compression and decompression of the tube. The drop in flow rate on the inlet and outlet precisely corresponds with the pressure pulses (flow rate drops overlap with pressure pulses). As expected, the flow rate even drops into negative values which coincides with the danger of reflux which is one of the main effects causing damage to blood cells. When we look at the course of the flow rate, we can see continuous drop during the compression and decompression that lasts a long time, relative to the duration of one revolution. Therefore, the mean value of flow rate is rather different than flow rate during the constant movement (for this particular case $Q_{mean} = 987\ \mathrm{ml/min}$ and $Q_{const} = 1360\ \mathrm{ml/min}$). The pulsation of the flow rate was not anticipated to be as problematic as it is implied by this figure a therefore was not part of the designing process. But for future research it would be beneficial to make the flow rate as constant as possible as the pressure pulsations are closely correlated to the flow rate.

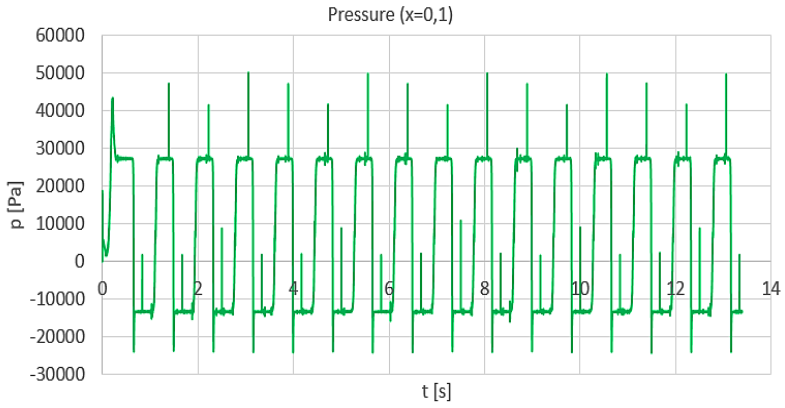

Figure 31 – Difference in pressure peaks during the periodic peristaltic pumping

As can be seen in Figure 31, one revolution was required to stabilize the simulation. When we look at the course of pressure closely, we can see that the peaks change with each revolution but are periodical when we look at three consecutive revolutions. Some changes in the amplitude of the peaks were anticipated but a difference as high as 9000 Pa for this particular setup is rather surprising. It would be best to wait for the experimental confirmation before we can draw any conclusion from this occurrence. Based on this difference in the pressure peaks, it is necessary to choose which peak will be used for the comparison between different setups. It was decided to use second peak as the first ones occur when the simulation is not yet stabilized, and it would require more computational time to compare peaks occurring later in the simulation. Similar pressure course was obtained from all the initial simulations and therefore the remaining simulations were carried out only for two revolutions.

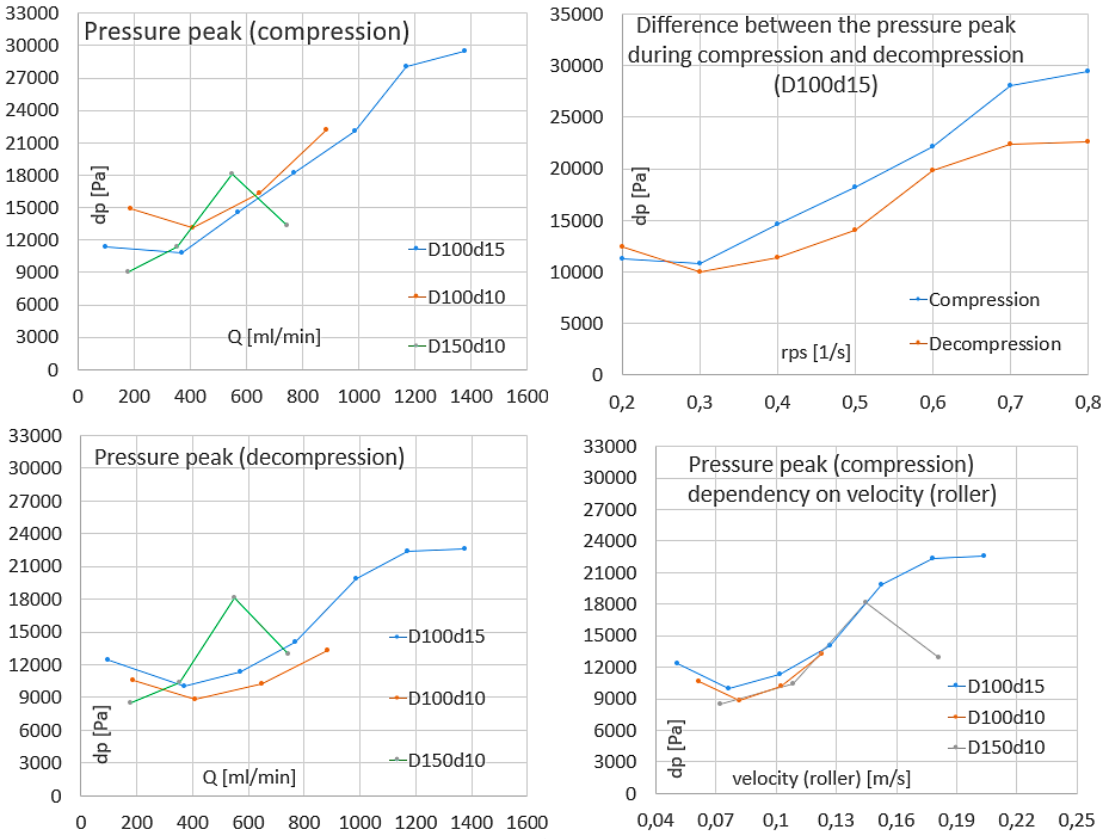

Figure 32 – Pressure peaks of compression (top left); Pressure peak of decompression (bottom left); Difference between the pressure peak during compression and decompression (top right); Dependency of pressure peaks on velocity of the roller (bottom right)

Based on Figure 32 it seems that compression will be more dangerous to blood than decompression, but when looking at experimental data from chapter 3 we can see that the pressure peak is higher for decompression. Data from the simulation are more likely to be incorrect and therefore we should be careful not to draw incorrect conclusions. For the purpose of the design both compression and decompression should be treated equally as a potential source of pressure pulsation. Additional information will be obtained from the experiment. On

the other hand, the dependency of the amplitude of the pressure peak on the flow rate turned out similar to the anticipated course. With increasing flow rate, the pressure peak rises.

As we can see in Figure 32 the pressure peak is very similar for all geometries. The differences are most likely caused by the simulation errors, thus no conclusion about the dependency of pressure rises on geometry of the tube can be drawn from the simulations. The pressure rise for flow rate of 350 ml/min is around 12 000 Pa for compression and 10 000 Pa for decompression. The dependency of the pressure rises on the velocity of the roller also did not provide any additional information. With increasing velocity, the pressure peak is higher, and the trend of the dependency is the same for all configurations. It is not conclusive whether the curve can be approximated by linear curve as both ends of the curve give the impression that they lead to some definite value. To prove this assumption more simulations, close to the zero value of flow rate, would have to be performed.

It is important to point out that the flow rate obtained from the simulations is vastly different than the theoretical flow rate calculated via equation (31). The difference can be seen in Figure 33. It was anticipated that the value from Ansys Fluent would be lower than the theoretical one because of the reversed flow through the gap near the bottom wall, which was not taken into consideration in the equation. Also, the reserved flow during the change in geometry should result into lower flow rate. Thus, the difference comes as a surprise and is not expected to be confirmed by the experiment.

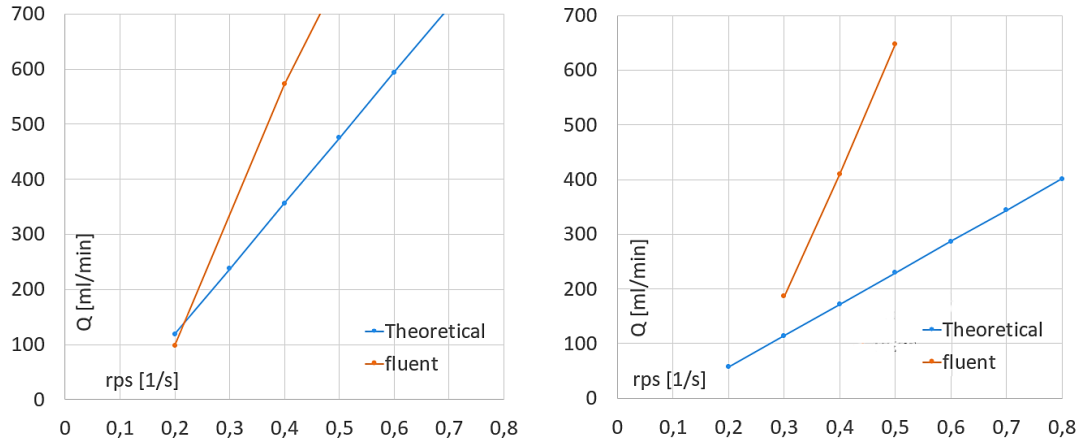

Figure 33 – Difference between theoretical flowrate and flowrate obtained from fluent; D100d15 (left); D100d10 (right)

In an attempt to make the simulation more precise the pulsating velocity profile obtained from pressure-pressure simulation was used as velocity inlet boundary condition. Although pulsating velocity inlet resembles actual character of the flow more closely, the outcome was inferior to the pressure-pressure boundary condition. The simulation was very unstable, so we were able to obtain data only for geometry D100d15. As can be seen in Figure 34 (inlet velocity and outlet pressure for rps 0,7), the pressure is fluctuating heavily with no apparent reasoning. During the second compression the pressure dropped to -250 000 Pa, which is well below legitimate physical limit as the pressure is relative to the atmospheric pressure (101 325 Pa). The pressure

for different rps had similar course and therefore it was decided that the calculations with inlet-pressure boundary conditions are inconclusive.

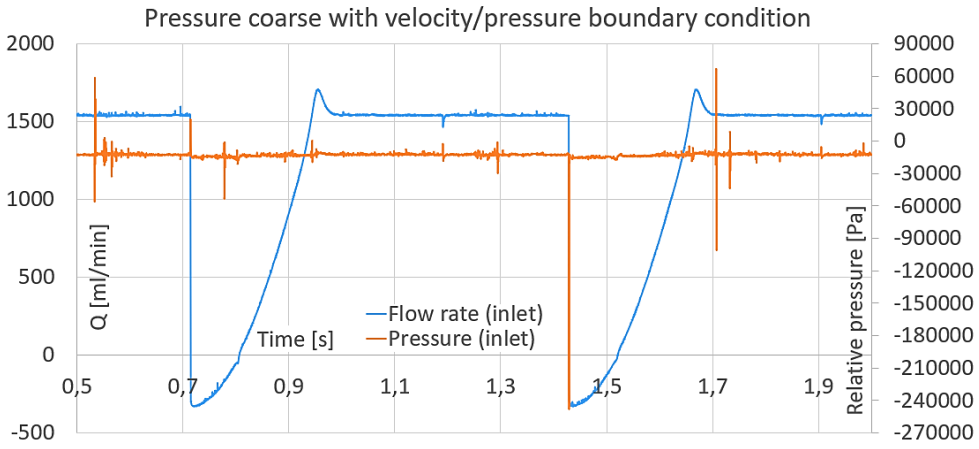

Figure 34 – Inlet flow rate and pressure coarse with velocity-pressure boundary conditions

Figure 35 represents the course of pressure and flow rate on inlet obtained from velocity-pressure simulations. We can see that with increasing flowrate the pressure slowly decreases. This means that with increasing flow rate the suction ability of the pump increases. It is important to remind that the results from velocity-pressure simulation were deemed inconclusive and therefore this information should be taken with extreme caution.

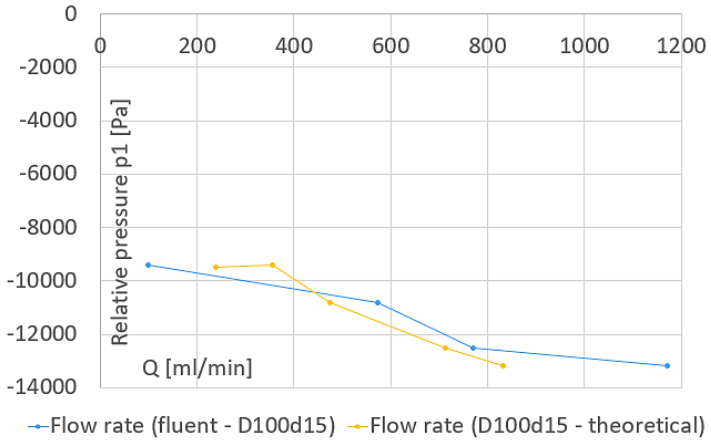

Figure 35 – Dependency of inlet pressure p1 on the flow rate

All the simulations (both with pressure-pressure and velocity-pressure boundary condition) were carried out with timestep equal to 0,0005 s. Smaller timestep (0,00001 s) was tried in order to improve the simulation, but the results' estimated accuracy was inferior to the original settings. However, smaller timestep appeared to be beneficial to avoid negative volume error during the compression of tube (most problematic moment of the entire simulation). It would be advantageous (especially for a more refined mesh) to include a changing timestep (function

DEFINE_DELTAT[5]) into the script. The calculation would switch to the smaller timestep during the deformation period and then switch back during the constant movement, resulting in shorter computational time while keeping the simulation less susceptible to negative volume error. As mentioned before, the same method could be applied to the remeshing interval, although it was not determined whether an appropriate function exists.

6.5 The second phase of simulations

In the second phase, the script prescribing the movement of peristaltic pump was adjusted to fit the 270° design from chapter 5.3.1. The script, for the most part, remained the same, except for the zones of compression and decompression that were adjusted, which resulted in prolonging the period of time when both rollers are compressing the tube. The inner diameter of the tubing is 13 mm, the diameter of the roller is 30 mm. The value of rpm was chosen to correspond with expected rpm during the experiment. The simulation was performed only for pressure-pressure boundary condition as previous simulations with velocity-pressure boundary condition did not prove to be advantageous.

Considering the surface, that has to be meshed, is larger for the final design than for the previously simulated geometries, the mesh has to be coarser in order to stay in the boundaries of student license. Fortunately, the coarser mesh did not have any impact on stability of the simulations and all the simulations were completed without any issues. The settings of the solver and of the dynamic mesh remained unchanged. The pressure course was measured on iso-surfaces in the distance (in the x_1 direction) of 0,15 and 0,35 m from the coordinate [0,0] as the iso-surface used in the first phase of simulations ($x_1 = 0{,}1\ m$) is not able to measure occurrences on outlet because the second roller is always between the iso-surface and the outlet.

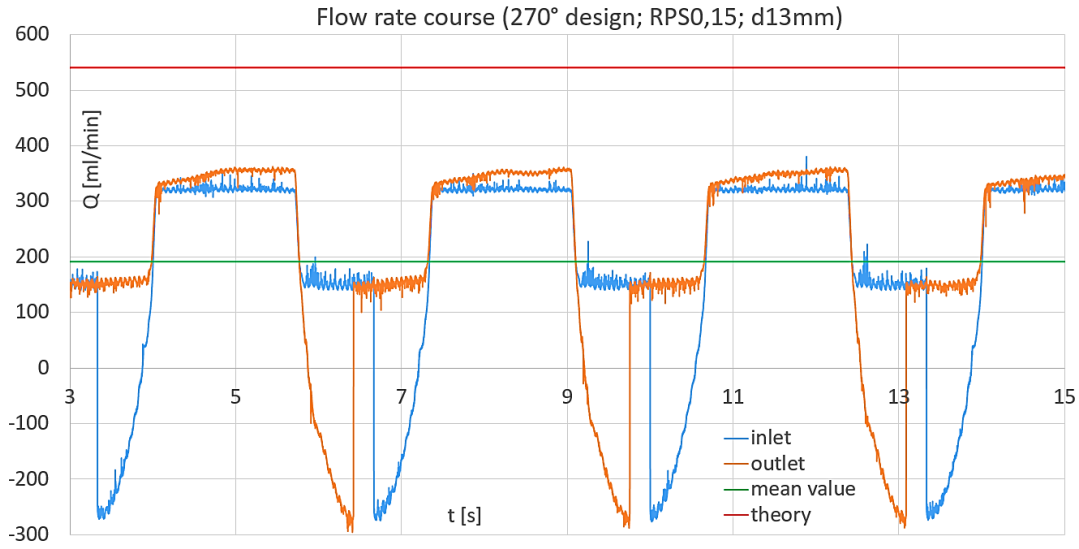

Figure 36 – Flow rate course (270° design; RPS = 0,15 1/s; d_{tube} = 13 mm)

[5] More information on variable timestep during the simulation can be seen in Fluent's manual.

In Figure 36 we can see flow rate course through inlet and outlet for simulation with $rps = 0{,}15\ s^{-1}$ as well as the values of theoretical flow rate and mean flow rate. When the second roller compresses the tube, reverse flow occurs in the tube that is followed by pressure rise in the same way as in the first phase of simulations with 180° concept. After the flow stabilizes, the flow rate is almost two times higher than when only one roller was moving the fluid through the tube. We can assume that the increase is caused by increased resistance against the reversed flow through the small occlusion gap. It can be assumed that the reverse flow rate in the simulation is higher than in reality, as the resistance is correlated to viscosity of the fluid which is lower in simulations than in reality. Additionally, the occurrences correlated to losses due to obstruction in the flow are reduced in 2D simulations (see equation (49)). Therefore, a dramatic rise in resistance, caused by the second roller, results in a more dramatic rise in flow rate for simulation compared to reality. On the other hand, the rise of flow rate is compensated by higher demands on engine of the pump as both rollers are compressing the tube.

When we compare the value of mean flow rate with theoretical flow rate (Figure 37), we can see that the mean simulated flow rate is lower, contrary to the results from the first phase of the simulation. The comparison of flow rates from the second phase is closer to the anticipated results as the trend of curves is more similar and the dependency on the rps appears to be linear. Flow rate obtained from experimental research is estimated to abide similar trend while being lower than theoretical results and higher than simulated results. The flow rate is reversed around the value $rps = 0{,}1\ s^{-1}$ where the pump is no longer able to propel blood through the circuit. It can be anticipated that the reversed flow is considerably lower in reality as the resistance of gap between the roller and supporting wall is notably lower in the simulation.

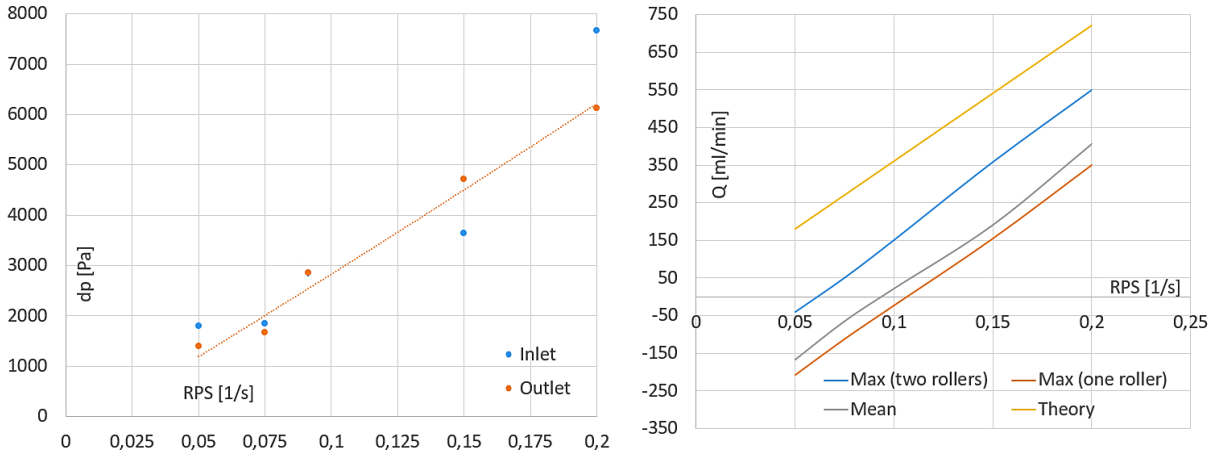

Figure 37 – Dependency of pressure rises on rps (left), dependency of flow rate on rps (right)

In Figure 38 the pressure course measured on two iso-surfaces can be seen. The pressure course is more oscillating than the pressure course from the first phase of simulations. We can see pressure rises corresponding to the compression and decompression but also pressure rises that cannot be easily explained. The more oscillating character of the flow is assumed to be occurring due to the fact that the iso-surfaces are sealed off from inlet and outlet constant

boundary condition which, as stated before, are expected to restrict pressure peaks during the simulation. Considering the pressure course did not drop below physically acceptable values and simulations were stable, we estimate that the character of pressure course will be similar to the pressure course obtained from experimental research. We can see that the pressure rises, corresponding to the reverse flow due to compression and decompression (marked in Figure 38), vary throughout revolutions but the difference is not as noticeable as it was during the first phase of simulations. The inlet pressure peaks are around 3600 Pa (the highest around 5800 Pa) and outlet pressure peaks around 4600 Pa (the highest around 6100 Pa.

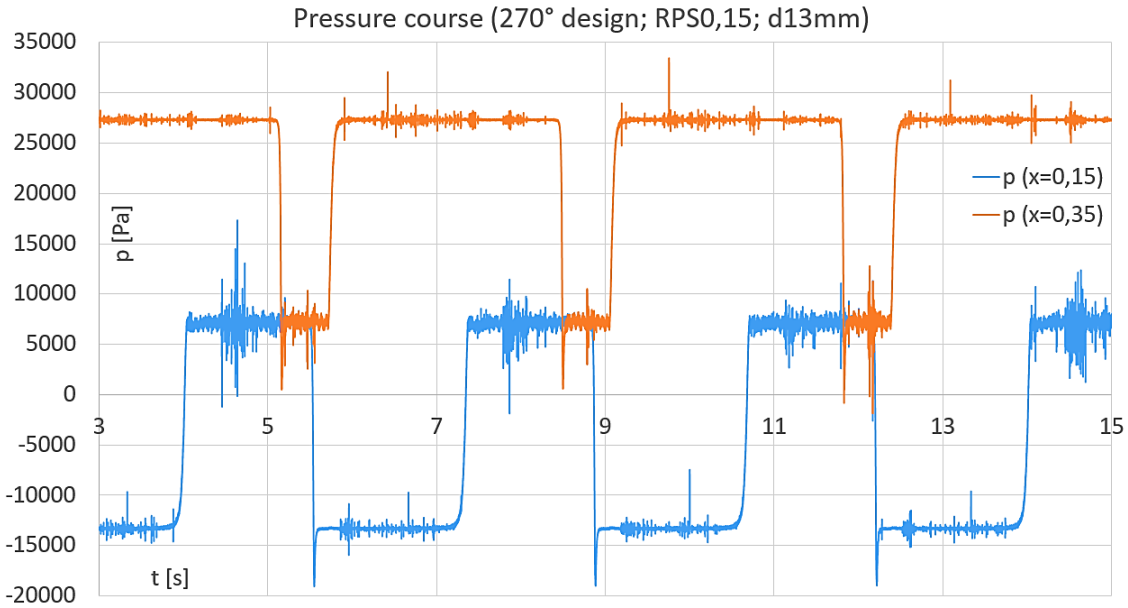

Figure 38 – pressure course (270° design; RPS = 0,15 $1/s$; d_{tube} = 13 mm

We can see that when both rollers are compressing the tube, the pressure rises in the volume between the rollers. The pressure in this volume is around 7000 Pa, which corresponds to the pressure rise of 20 300 Pa, and is constant for all values of rps. Even though pressure rise in this volume was anticipated, simulated rise is estimated to be too high. Considering the value remains the same for all variants of rps, the rise is dependent on geometry of the tube. A few simulations were carried out with smaller diameters of the tube to prove this assumption. The results confirmed that the pressure rise changes with different diameters and remains the same with different values of rps and is therefore most likely caused by the reduction of volume in which the fluid is contained. It is important to point out that only a few simulations were carried out due to limited amount of time, thus this information should be taken with caution.

If pressure rise of this magnitude proved to be correct by experimental analysis (which is unlikely), it would mean that 270° shape of the pump would in itself provide protection against the reversed flow as the pressure difference in front of and behind the roller would be lower. It is not possible to compare simulation with its 180° counterpart because no simulation with similar geometry was carried out during the first phase and the results would most likely vary

due to a problem with pressure boundary condition (as explained before). Unfortunately, the pressure in the volume between rollers is difficult to measure during experimental analysis and therefore this effect of 270° concept will most likely not be confirmed.

The dependency of pressure rises on flow rate can be seen in Figure 37. While pressure rises on the outlet correspond with linear regression, it cannot be determined whether pressure rises on the inlet correspond with linear, quadratic or exponential regression. Based on Figure 32, obtained in phase one, and the fact that pressure rises on inlet and outlet are likely correlated, we assume that the regression is linear, but more simulations have to be carried out to prove this hypothesis. It is important to point out that the trend of pressure rises remains consistent even for rps where the pump is no longer able to push blood through the system.

6.5 The third phase of simulations

The aim of the third stage is to incorporate the idea of variable acceleration from the second design into the simulations, thus getting confirmation that the acceleration of the second roller indeed does lead to increase in pressure in the volume between the rollers. Unfortunately, the attempts to adjust the script were not successful and therefore the third stage was not completed. Thus, the following chapter serves as summary of findings that outline the main issues that need to be overcome in future research.

The main complication that is important to overcome is the storage of values between timesteps. As movement is prescribed to the control point C, an entity that exist only in the script and does not have a real representation in Ansys Fluent, the coordinates of point C are not stored in the memory of Ansys Fluent to the next timestep and have to be calculated at the beginning of each timestep as a function of time. The trajectory of point C is prescribed before the start of the simulation and therefore it is easy to determine the stages of movement (explained in chapter 6.3) and velocity as it remains constant through the simulation. Thus, it is manageable to define its movement in the script without the need to store coordinates of points C between timesteps.

The movement along the elliptic casing is way more challenging. The stages of movement (the position where the tube starts to compress/decompress) are still easy to calculate but the variable movement is not, because the change in velocity is immediately projected into the trajectory that was already travelled by control point C, resulting in a sudden skip in the position. The skip usually results in a negative volume error, but even if it did not, the movement would still not accurately correspond with the movement of the roller.

A possible solution to this problem is to calculate the velocity based on the distance from the center of rotation for each timestep and add the increment of distance travelled during the timestep to the position of point C that will be stored in Ansys memory till the next timestep. The UDF F_UDMI [37] is able to access and store user-defined memory on a faces (it is often used to store temperature value of the wall till the next timestep), therefore it should be possible to store the coordinates of each control point and retrieve it in the next timestep. Unfortunately,

while the function seems simple enough to incorporate into the script based on Ansys Fluent manual, all the attempts were unsuccessful.

```
/* Compute face temperature and store in user-defined memory  */
begin_f_loop(f,t)
  {
    temp = F_T(f,t);
    F_UDMI(f,t,0) = (temp - tmin) / (tmax-tmin);
  }
end_f_loop(f,t)
}
```

Figure 39 – Example of F_UDMI (storage of temperature in user-defined memory) [37]

In order to store values in Ansys Fluent memory, it is first required to allocate appropriate number of memory location(s) in the User-defined Memory panel. [37] By doing so a variable called *"User Memory i"* (where i is a number between 0 and 500) is created for every user-defined memory location that is stored between timesteps. It is anticipated that the problem lays in allocation of memory and not in the usage of F_UDMI UDF, but we were unable to determine the character of the error any further.

If the problem of variable memory storage was overcome, it would result in an immediate improvement of the scrip, even for the previous two phases, as almost half of the lines of the code are used to bypass this inconvenience. This would result in a performance improvement that is especially necessary if the code should be improved with more refined mesh and smaller timestep.

7. Experiment

The following chapter describes the experimental analysis of the manufactured peristaltic pump. The experiment is an important part of the designing process as the numerical simulation is often used to obtain relative values for comparison of various options but is less trusted when providing information about magnitude of variables. Furthermore, experimental data can be used to improve the simulation models by providing more accurate boundary conditions.

In the first part of this chapter, the experimental circuit and procedure is described, as well as the adjustments made to the peristaltic pump prior to the experiment. Information on measured quantities, measuring equipment and equations for the calculations with measurement of uncertainty follow. The last part of the chapter is dedicated to the results and comparison between the experimental and simulated data.

7.1 Description of the experiment

The experiment was divided into two parts. In the first part, the experiment was carried out with the initially planned tygon tube and the engine with parameters in the range of calculated values from chapter 5.2. In the second part, due to unsatisfactory behavior of the tygon tube and engine, the experiment was adjusted and performed with a tube which is being used for hemodialysis at Saint Ann's hospital in Brno. The engine was replaced with a lathe.

The experimental circuits followed the same concept for each variant (see Figure 40). Only the height of the cannisters (in reference to the pump) changed to set different pressure on the suction and pressure side of the pump. The pressure course was measured in front of and behind the pump by pressure sensors listed in chapter 7.1. The shaft of the engine was connected to the engine and the torque was measured by a tensometric shaft. A valve was positioned in front of the pressure side cannister for regulation. The information from sensors were processed in labview and saved to a text file for future evaluation.

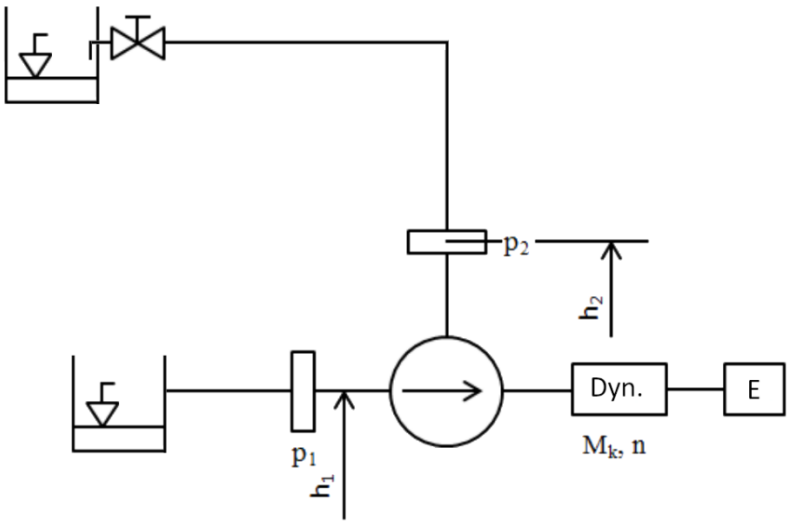

Figure 40 – Scheme of the experimental circuit

As mentioned before, the first measurement with tygon tube did not provide sufficient information, therefore the second part of the measurement was carried out with different tubing which was predicted to improve the functioning of the pump. Unfortunately, this tubing required higher value of torque which resulted into slip between the shaft and the connecting parts. To overcome this complication, it was decided to use lathe as an engine for the pump which meant not being able to sufficiently measure the torque on the shaft which results in inability to determine efficiency of the pump. Photos of each experimental circuit are enclosed in the appendix.

Before the experiment an adjustment had to be made to the pump. The roller had to be enlarged, otherwise the pump would not seal the tube correctly which would have resulted into reversed flow from the pressure side to the suction side when the pump is not operational. Because the occlusion was set based on recommended range, slight changes to the final design were anticipated.

7.3 Measurement information

The following chapter contains all the information necessary for the completion of the experimental analysis – a list of measured quantities, a list of measuring equipment, equations for calculations of required quantities and equations for measurement uncertainties. The calculations can be seen in the Excel file in the appendix.

Measured quantities:

- p_1 – suction-side pressure kPa
- p_2 – pressure-side pressure kPa
- M_k – torque Nm
- n – revolutions per minute min^{-1}
- Q – flow rate $ml \cdot s^{-1}$

Measuring equipment:

- p_1 – pressure sensor DMP 331, manufacturer BD SENZORS s.r.o. Uh. Hradiště, range 0 – 2,5 bar (A), measurement accuracy ±0,25 % from range, output 0–20 mA, v.n. 111160122
- p_2 – pressure sensor DMP 331, manufacturer BD SENZORS s.r.o. Uh. Hradiště, range 0 – 2,5 bar (A), measurement accuracy ±0,25 % from range, output 0–20 mA, v.n. 111160122
- Mk, n – tensometric shaft TM 208 HS, manufacturer Vibro-Meter, range of torque 0 – 20 N·m, range of rpm 0 – 50000 min-1, accuracy ±0,001 of range, frequency output, output 30 pulses per minute, v.č. 415-208-000-111
- Q – Considering the flow rate pulses are difficult to measure, only mean value of the flow rate was measured. Time was tracked during the filling of the canister. The cannister was then measured on a weighing scale to obtain the value of flow rate. This

procedure was repeated 5 times and the final value was defined as the calculated average value.

Calculations of required quantities:

Besides the pressure course on inlet and outlet, it is necessary to determine the efficiency of the pump. The following equations are required for the calculations.

Hydraulic energy:

$$Y = \frac{p_2 - p_1}{\rho} + g\Delta\mathrm{h} \tag{51}$$

Output of the engine calculated from the torque on the shaft:

$$P_e = 2\pi n M_k \tag{52}$$

Efficiency:

$$\eta = \frac{\rho Q Y}{P_e} = \frac{\rho Q Y}{2\pi n M_k} \tag{53}$$

Measurement uncertainties:

An important part of the experiment is to determine the uncertainty of the measurement. The measurement uncertainty is carried out only for systematic uncertainty (type B), which corresponds to the uncertainty of the measurement equipment. The measurement uncertainty can be determined as follows:

$$u_{BY} = \sqrt{\left(\frac{u_{Bp2}}{\rho}\right)^2 + \left(\frac{u_{Bp1}}{\rho}\right)^2 + \left(\frac{u_{BQ}\cdot \mathrm{Q}}{\mathrm{S}_2^2}\right)^2} \tag{54}$$

$$u_{B\eta} = \sqrt{\left(\frac{\rho\cdot \mathrm{Q}}{P_M}\cdot u_{BY}\right)^2 + \left(\frac{\rho\cdot \mathrm{Y}}{P_M}\cdot u_{BQ}\right)^2 + \left(\frac{\rho\cdot \mathrm{Q}\cdot \mathrm{Y}}{P_M^2}\cdot u_{BP_e}\right)^2} \tag{55}$$

The uncertainty of engine output can be calculated as follows:

$$u_{BPe} = \sqrt{\left(\frac{\partial P_e}{\partial M_k}\right)^2 u_{BM_k} + \left(\frac{\partial P_e}{\partial n}\right)^2 u_{Bn}}, \tag{56}$$

which can be further adjusted to the following equation:

$$u_{BPe} = \sqrt{\left(2\pi n u_{BM_K}\right)^2 + (2\pi M_k u_{Bn})^2} \tag{57}$$

Unfortunately, the uncertainty of flow rate cannot be determined because the measurement was performed by an inaccurate method of weighting the cannister while tracking the time. The uncertainties of other parameters are negligible in comparison with the uncertainty of the flow

rate. Because the efficiency is a function of flow rate, it is not possible to accurately determine the uncertainty. Only pressure uncertainty can be properly determined (see MS Excel in the appendix for specific value)

7.4 Results

The experiment is divided into two parts. The first part did not provide any valid data for the comparison with the simulations, but clarified the issues connected to the design. In the second part, the issues were overcome by replacing tygon tube for tubing used for hemodialysis by Saint Ann's hospital in Brno and substituting the engine for the lathe.

7.4.1 The first part of the experiment

Results of the first part of the experiment are unsatisfactory as the tygon tube proved to be unusable for the peristaltic pump. The course of pressure and torque can be seen in Figure 41 and Figure 42. The main problem is that the tube does not decompress in the volume between the rollers and therefore the flow rate is considerably lower as less liquid is transported with each revolution. The pump rotates at 12 rpm which corresponds to the theoretical flow rate of 720,5 ml/min, but the actual flowrate is around 340 ml/min. With higher pressure difference between pressure and suction side, the flow rate drops even lower (around 100 ml/min). Furthermore, as the tube does not maintain its original shape, the support rollers do not fulfill their function and the tube is free to move in the pump which results in even more losses in the system as the tube is not accurately compressed. To overcome this problem, a different tube was used for the second experiment.

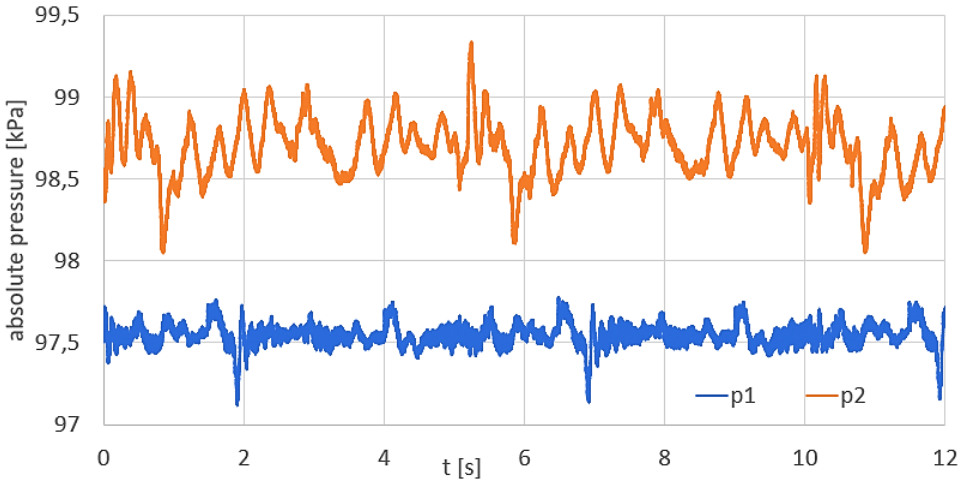

Figure 41 – Pressure course on inlet and outlet for the experiment with tygon tube

The second considerable issue with the design is that the connections between the shaft, the tensometric sensor and the engine slip with higher values of torque even though the engine in itself is powerful enough to supply the pump. Therefore, it is not possible to provide the necessary torque and the pump does not operate smoothly and is prompt to seizing up.

Due to insufficient torque to pump is measured only for low differences of pressure which results in very low efficiency (around 1,8 %) because most of the torque is used for the compression. To get a better understanding of the percentage of the power, that is lost in the compression, the pump was measured without water in the tubing. The course of the torque with and without water can be seen in Figure 42 (data with and without water are not synchronized in time). The torque required for decompression is almost 83 % of the entire torque (0,57 Nm) measured during operation of the pump. It is important to point out, that the torque required for compression is higher when water is propelled through the pump and therefore the losses are even higher. The value of torque for decompression does not change drastically with higher pressure difference in front of and behind the pump, so the low value of efficiency is not as troublesome as first anticipated.

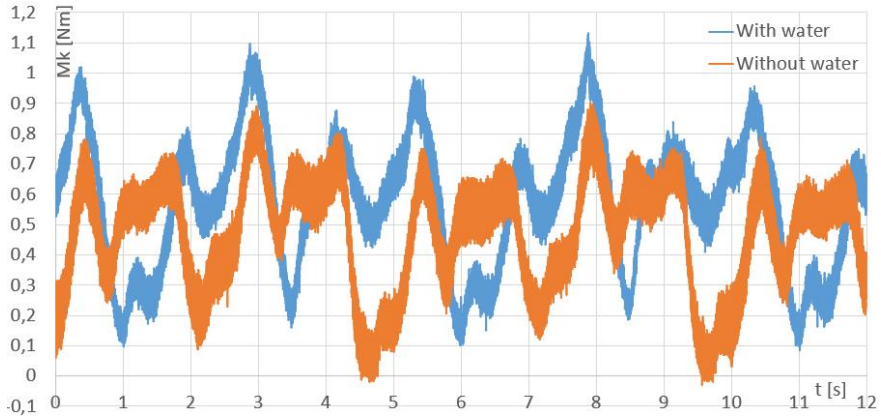

Figure 42 – Difference in torque course between the operation with and without water

If the connections of the shaft allowed higher torque, the additional power would be used to propel the fluid, not lost on compression, which would result in higher efficiency. To continue with the experiment, other option for the engine needs to be devised, that will not use insufficient connections for the shaft. The solution of this problem is a lathe that does not need connections for the shaft but is unable to measure torque. Therefore, only pressure sensors will be used for the second part of the experiment.

7.4.2 The second part of the experiment

The experimental circuit for the second part of the experiment is adjusted to fit the pressure boundary conditions from the simulations as closely as possible. The pressure in front of the pump is 86,4 kPa and pressure behind the pump is 129,2 kPa. The pressure is obtained by positioning the suction cannister on the ground (approximately 115 cm under the level of the pump) and pulling the pressure cannister by the crane approximately 280 cm above the level of the pump. The precise pressure difference is measured by pressure sensors while the pump is not running. The torque is provided by a lathe, which is able to regulate rpm, therefore it is possible to create characteristic of the designed pump. The pump is measured for rpm of 6; 10,2; 13,5; 17,6 and 20,7.

Instead of the original tygon tube, the tube, used by Saint Ann's hospital in Brno for hemodialysis, is utilized. Unfortunately, it is not possible to provide any additional information about the tube (besides the size parameters), due to limited amount of time left for the experiment. The inner diameter of the tube is 9 mm and thickness of the wall is 2 mm. This tube proved to be a far better option, as it did maintain its shape even under compression. Contrary to the first attempt, the support rollers proved to be a valuable part of the pump as only two rollers were unable to maintain stiff tube in the contact with the casing. If it was not for the support rollers, the tube would not go along the casing which would result in smaller volume between rollers, thus lower flow rate. It would be better to adapt the design to having 6 support rollers to further prevent the tube from shifting.

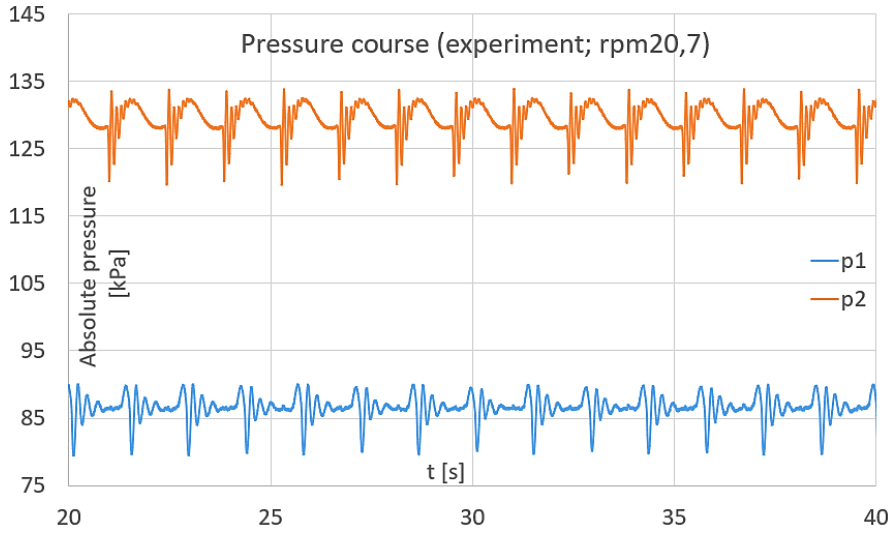

Figure 43 – Example of experimentally obtained pressure course

As an example of pressure course (rpm 20,7) can be seen in Figure 43. We can see pressure rises on the inlet and outlet that correspond with compression and decompression. The frequency of pressure rises is equal to the rpm of the pump. In Figure 44 the characteristic of the pump can be seen as well as the dependency of pressure rises on flow rate for inlet and outlet. It is apparent from the characteristic that the hydraulic energy is not dependent on flow rate which corresponds to the characteristic of volumetric pump. A better representation is the dependency of flow rate on rpm (respectively rps) where we can see the difference in theoretical, experimental and simulated flow rate (see Chapter 7.5). On the right side of Figure 44 we can see that the pressure rises on the outlet can be interpolated by a linear function. As for the inlet's pressure rises the dependency is not as clear as for the outlet but based on the assumption that both pressure rises are correlated, the linear function was used for interpolation. To further supplement this assumption, the pump should be experimentally measured for lower values of flow rates.

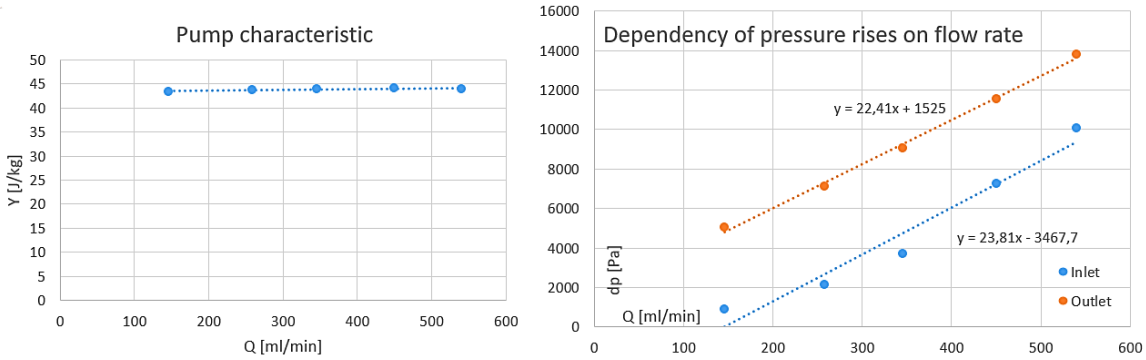

Figure 44 – Pump characteristic (left), Dependency of pressure rises on flow rate from the experiment (right)

7.5 Comparison with simulations

Since the tygon tubing had to be replaced by more suitable tubing, it is necessary to convert the values from Ansys Fluent to correspond with smaller volume between rollers. Simulated flow rate was therefore multiplied by the ratio of volumes. It is important to point out that the pressure rises can be dependent on the geometry of the tubing and therefore this conversion might be inaccurate, nevertheless it is the only option that enables for comparison. It would be beneficial to repeat the simulations to get a better idea of validity of this conversion.

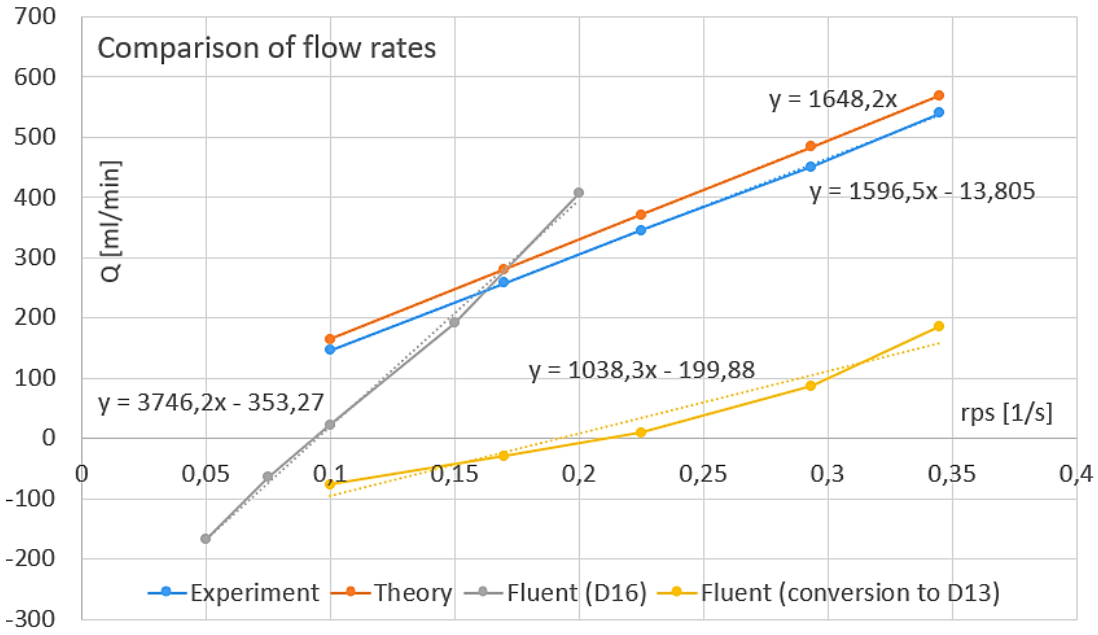

Figure 45 – Final comparison of flow rates

Final comparison of theoretical, experimental and simulated flow rate can be seen in Figure 45. Based on this figure, we can see that the experiment corresponds with the theoretical values with hydraulic efficiency between 89 and 95 %. The efficiency is increasing with increasing flowrate. After the conversion of the simulated values, the trends of the curves are similar, but the value of simulated flow rate is considerably lower. The simulated values even continue to

negative values which is unlikely for the experimental values, if the pump functions properly, as the occlusion gap is small enough to efficiently seal the tube. As was already mentioned before, this difference is caused by insufficient modeling of resistance (losses) for simulated values, especially for 2D simulations with coarse mesh.

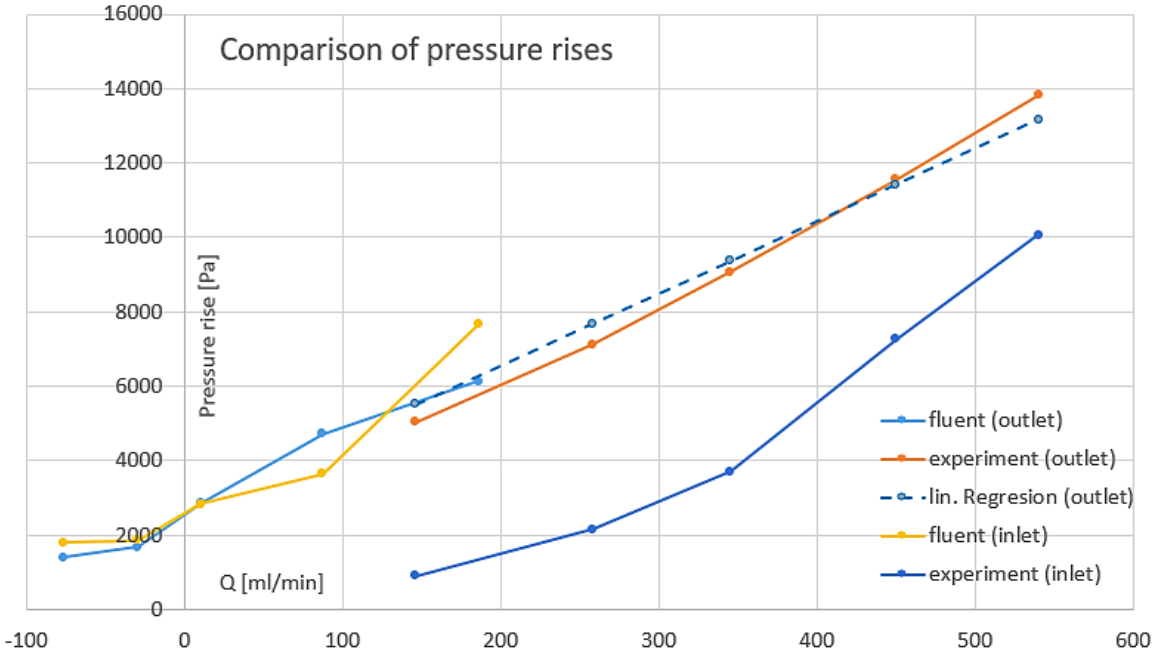

Figure 46- Final comparison of pressure rises

The converted simulated flow rate demonstrates promising results as the trend is similar to experimental values and therefore the same compression is carried out for comparison of pressure rises (see Figure 46). Unfortunately, the simulations were performed for lower ranges of flow rates because it the usage of tygon tube was anticipated for the experiment. Despite this fact, the comparison between experimental and simulated values shows promising results. The curve, calculated by equation from linear regression of the outlet pressure rises, correlates strongly with experimental values. The difference ranges from 1,29 to 9,29 % (in relation to the experimental values), which corresponds to pressure difference between 160 to 650 Pa. The pressure rises on the inlet do not look as promising as they show higher similarity with outlet experimental values. Generally, the difference between inlet and outlet is not as marginal for the simulation as it is for the experiment.

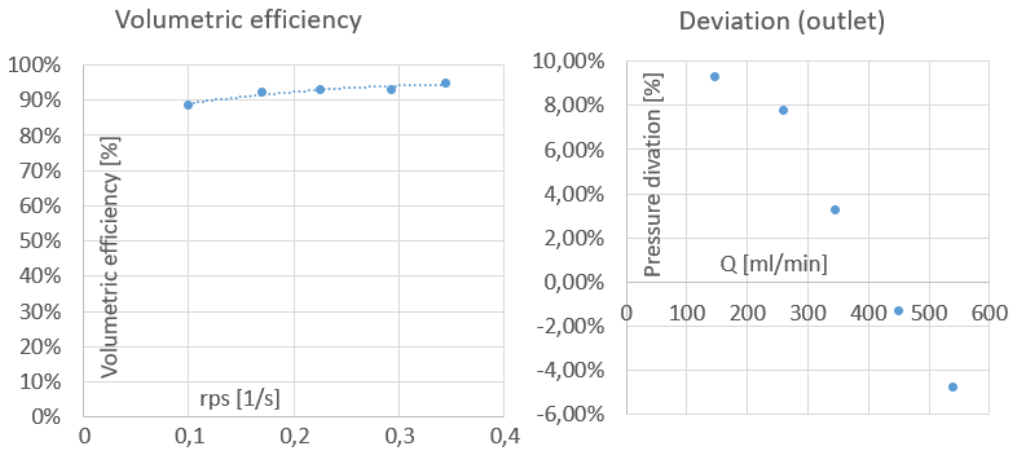

Figure 47 – Dependency of volumetric efficiency on rps (left), deviation of pressure rises on the outlet (right)

Considering all the simplification of the simulations, differences between simulation geometries and the final design and measurement uncertainty, the deviation is lower than anticipated. More simulations with current settings and more experimental measurements should be carried out to confirm the correctness of the simulation model (see Chapter 8 for the discussion). Figure 47 shows the hydraulic efficiency and the deviations for the pressure rises.

8. Discussion

In the following chapter, the results as well as main issues and recommendations are discussed.

The 270° concept from analytical analysis proved to be suitable with the "basic" setup without acceleration which was confirmed by the experimental analysis. Unfortunately, the focus dedicated to the material of the tubing, which proved to be a major parameter of the design, was not sufficient. Even though the importance of a properly chosen material for the tube was known based on literary research, the tubing was considered to be suitable as it is used by Department of Fluid Engineering at Brno University of Technology for experiments linked to blood flow due to its compatibility with blood. It was therefore assumed that it can be used in peristaltic pump as well, which proved to be incorrect as the material was unable to maintain its shape when compressed by rollers. The deformed shape resulted in lower volume between the rollers as well as shifting of the tube which led to poor volumetric efficiency. All the problems with the operation of the pump were resolved by replacing the tubing for a variant used by Saint Ann's hospital in Brno.

The operation of peristaltic pump is closely tied to deformation of the tube which was not the main focus of this thesis. To further improve the design, thorough analysis of the peristaltic pump movement deformation is required. A smoother deformation during compression and decompression are anticipated to result in better efficiency and lower pressure pulsation.

The support rollers proved to be an invaluable part of the design as the tube does not maintain shape identical to the curvature of the casing, therefore the volume between rollers is decreased which results in lower values of volumetric efficiency. The guidance provided by the rollers allows the tube to correspond with its intended circular trajectory more closely. The rollers function sufficiently even for tubes with smaller diameters. For the current design, an optimal number is at least six support rollers. Furthermore, it is necessary to optimize the current design with contracting attachment on inlet and outlet of the casing, as the tubing with smaller diameter than anticipated is pulled inward the pump.

Besides these complications, the pump was able to supply the required pressure difference into the circuit, but due to the use of a lathe instead of the engine, no data of torque were acquired to confirm the estimation of the required parameters of the pump. If better connections between the shaft and engine are provided, it would be advantageous to repeat the experiment while measuring the torque. Based on the value of the torque measured without water, it seems that the estimation was, as anticipated, exaggerated.

Despite all the simplifications and issues with simulations with dynamic mesh, the numerical model proved to accurately predict pressure rises on outlet as was verified from the experiment. The pressure rises on inlet show significant differences in magnitude and are closer to the values on outlet. Unlike the experiment, the simulation does not show significant disparity between pressure rises on inlet and outlet. The differences between experimentally obtained flow rate

and theoretical flow rate is between 5 % and 10 %. The simulated values show similar trend as theoretical and experimental values, but the magnitude is vastly different. Possible reasons for the discrepancy are discussed below.

To further improve the 2D model, it is necessary to solve the problem of occlusion gap which evince lower resistance to the flow than reality, shown by experimental data. A possible direction for improvement is performing simulations for various values of occlusion gap and, based on the comparison with experiment, use the value that shows the highest similarity with the experiment. Unfortunately, this direction will most likely result in finer mesh because of the necessity to place at least three cells between the walls to ensure the calculation of velocity profile. Furthermore, the curvature nature of the peristaltic pump can be included into the model and the function controlling the deformation can be set more accurately. The curvature nature could prove to be difficult to incorporate into the simulations and it most likely does not have significant impact on the results, but further research is needed to confirm this hypothesis.

The second significant inconvenience are boundary conditions. Through the simulations, it became apparent that inlet-pressure boundary condition is not very stable, as the inlet boundary condition has to be almost identical to the flow rate caused by the peristaltic movement prescribed by UDF. Unfortunately, pressure-pressure boundary condition proved to reduce the pressure pulsation in the system, thus it is not possible to obtain pressure values from inlet and outlet. The values have to be obtained from the volume between rollers, and therefore the comparison of pressure courses between experiment and simulations cannot be done. It could be possible to use data from experimental analysis to predict the nature of the flow rate boundary condition more accurately, but experimental measurement of transient flow rate is in itself a complicated task.

Another option for improvement is connected to the inability of Ansys Fluent to properly simulate vortices within 2D model. A 3D simulation would provide more accurate results but the requirements on computational power and complexity of the script would rapidly increase, thus 3D simulation with defined wall deformation within the UDF is not a convenient option. A better option is to perform the calculation as Fluid Structure Interaction, which would provide a possibility to see the impact of pressure pulsation on the deformation of the wall, which is not possible with current 2D simulation because Ansys Fluent does not support FSI in 2D. Even though FSI would most likely result in more accurate prediction of the flow, it is more convenient to further improve current 2D model and use FSI only at the end stages of development.

The elliptical design, devised parallel to the "basic" design, requires further research. Even though the analytical analysis indicates a connection between the acceleration of the roller and the increase of pressure in the volume between rollers, experimental analysis is required to prove this hypothesis. The numerical simulation can be used to partly verify the hypothesis, but we were unable to adjust the simulation model to correspond with the elliptical design.

The most prominent direction of future improvement is function UDMI that allows the storage of variables through timesteps. Successful implementation would result in immediate improvement of the script, even for the prior simulations, as almost half of the script is used to overcome this problem. Therefore, this implementation needs to be the main focus of any future improvement of the 2D simulation model. After successful utilization of UDMI, the adjustments to the code to fit the elliptical design are straightforward. The simulation model could be, as stated before, used to partly confirm the hypothesis and also to predict the optimal acceleration for the reduction of pressure pulsation.

If the idea is proved to be applicable, the research can switch focus to the best design of the pump. It would be beneficial to design the pump without the need of a control unit, meaning that only variable distance between center of the rotation and the center of the roller would be used. Possible options include elliptical casing with pneumatic or mechanical springs, and kinematic arms. The possibility of a sliding arm, mentioned in chapter 5.3.1, can be also explored.

9. Conclusion

The main objective of this thesis was to investigate blood flow in peristaltic pumps, with emphasis on reduction of pressure pulses caused by compression and decompression of flexible tubing inside the pump. Furthermore, based on information obtained by analytical analysis and numerical simulations, the goal was to design a working peristaltic pump that utilizes proposed modifications leading to reduction of pressure pulses. Additionally, the aim was to create a numerical model in Ansys Fluent that can simulate the peristaltic pump's operation and efficiently predict the dependency of pressure pulses on various parameters of the pump.

Through analytical analysis a new concept for the reduction of pressure pulses was devised. This concept uses acceleration of the second roller to increase the pressure in the volume between rollers, which results in a lower pressure difference in front of and behind the exiting roller. Lower pressure difference is predicted to lead to lower pressure pulses on outlet, since flow reflux is decreased. Possible working designs for the concept were introduced, but we were unable to manufacture a working prototype to confirm the hypothesis by an experiment and therefore the completion of the design remains subject for future research.

Parallel to the new concept, a more traditional pump was designed and manufactured with the purpose to obtain more information for the improvement of the new concept. The more traditional design utilized "270° trajectory" of the tube, an idea, that should enable more continuous acceleration of the roller.

Experimental analyses proved that the pump is able to supply required pressure difference and flow rate with volumetric efficiency above 90 % and pressure rises around 9 kPa (outlet) and 4 kPa (inlet). Unfortunately, the measurement of torque was not possible due to slip in connections with tensometric shaft and therefore the values of efficiency were not determined. Additionally, the experiment highlighted the importance of sufficient material of the tubing, as tygon tube proved to be inapplicable, due to inability to maintain its shape when compressed by rollers, which resulted in decrease of volume between rollers (corresponding with decrease in volumetric efficiency). The experiment had to be carried out with unanticipated tube used by Saint Ann's hospital in Brno. The experiment also proved the necessity of support rollers or other fixing components, otherwise the tube does not follow the curvature shape of the casing. This is especially true for the "270° concept". At least six support rollers need to be used for the current design.

Using Ansys Fluent a 2D numerical model of peristaltic pump operation was created. Dependency of pressure rises on various parameters of the pump was calculated and based on these values a linear function corresponding with pressure rises on outlet obtained by the experiment was interpolated. The 2D model was able to predict dependency of pressure rises on flow rate on outlet with deviation ranging between 1 % and 7 %. The deviation for inlet was more severe as simulated pressure rises on inlet and outlet are almost identical in magnitude, while experiment shows difference between the pressure pulses on inlet and outlet. Even though

more simulations and experiments have to be carried out to confirm this result, the simulation model can be used to quickly validate the influence of various parameters of the pump on magnitude of pressure rises.

The concept with acceleration could not be simulated as the issue of transferable variables through timesteps has to be overcome first. A solution of this issue is most likely connected to User Defined Memory in Ansys Fluent which would result in considerable improvement to the script defining the deformation of the wall during simulation. In the end stages of the development process it would be advantageous to simulate the peristaltic pump as Fluid Structure Interaction which would provide the most accurate results.

References

[1] WOLFE, Robert A., Valarie B. ASHBY, Edgar L. MILFORD, Akinlolu O. OJO, Robert E. ETTENGER, Lawrence Y.C. AGODOA, Philip J. HELD a Friedrich K. PORT. Comparison of Mortality in All Patients on Dialysis, Patients on Dialysis Awaiting Transplantation, and Recipients of a First Cadaveric Transplant. *New England Journal of Medicine*. 1999, **341**(23), 1725-1730. DOI: 10.1056/NEJM199912023412303. ISSN 0028-4793.

[2] MARKOVIC, Miroslav, Michael RAPIN, Marc CORREVON a Yves PERRIARD. Design and Optimization of a Blood Pump for A Wearable Artificial Kidney Device. *IEEE Transactions on Industry Applications*. 2013, **49**(5), 2053-2060. DOI: 10.1109/TIA.2013.2260851. ISSN 0093-9994. Available at: http://ieeexplore.ieee.org/document/6513240/

[3] *Hemodialýza* [online]. Praha: Magdaléna Mokrješová [cit. 2019-05-23]. Dostupné z: https://slideplayer.cz/slide/3085254/

[4] LYSAGHT, MICHAEL J. Maintenance Dialysis Population Dynamics: Current Trends and Long-Term Implications. *Journal of the American Society of Nephrology*. 2002(13), 37-40.

[5] KNIGHT, Christopher J. *The Development of an Artificial Heart Valve*. Edinburg, 1973. Thesis submitted for a degree of Doctor of Philosophy. University of Edinburg. Supervisor Dr. Norman Wacleod.

[6] OLSON, Jeffrey Carter. *Design and modeling of portable hemodialysis system*. Georgia, 2009. Dissertation thesis. Georgia Institue of Technology. Supervisor Dr. David Rosen.

[7] TORTORA, Gerard J. a Bryan DERRICKSON. *Principles of anatomy and physiology*. 14th edition. Hoboken: Wiley, [2014]. ISBN 978-1-118-80843-6.

[8] IBRAHIM, Hassan N., Robert FOLEY, LiPing TAN, Tyson ROGERS, Robert F. BAILEY, Hongfei GUO, Cynthia R. GROSS a Arthur J. MATAS. Long-Term Consequences of Kidney Donation. *New England Journal of Medicine*. 2009, **360**(5), 459-469.DOI: 10.1056/ NEJMoa0804883. ISSN 0028-4793.

[9] Renal transplant. In: *Https://nephrology.medicine.ufl.edu/patient-care/ research/transplant/* [online]. Florida [cit. 2019-05-20]. Available at: http://com-dom-neph.sites.medinfo.ufl.edu/files /2011/12/tranplantclinic.jpg.

[10] SCHALL, John A. A New Outlook on Compensated Kidney Donations. *RENALIFE: American Association of Kidney Patients*. 2008.

[11] *Náhrada funkce ledvin* [online]. [cit. 2019-05-20]. Available at: https://www.wikiskripta.eu/w/Náhrada_funkce_ledvin.

[12] FORNI, L.G. a P.J. HILTON. Continuous Hemofiltration in the Treatment of Acute Renal Failure. *New England Journal of Medicine*. 1997, **336**(18), 1303-1309. DOI: 10.1056/NEJM199705013361807. ISSN 0028-4793.

[13] *Email communication with Saint Ann's hospital in Brno,* Brno, 2019

[14] *Email communication with* MUDr. Martin Havrda, Brno, 2019

[15] MITRA, Sandip a Nicos MITSIDES. Technical Aspects of Hemodialysis. *Core Concepts in Dialysis and Continuous Therapies*. Boston, MA: Springer US, 2016, 2016-06-14, , 15-26. DOI: 10.1007/978-1-4899-7657-4_2. ISBN 978-1-4899-7655-0. Available at: http://link.springer.com/10.1007/978-1-4899-7657-4_2

[16] MANSOR, Mohd Firdaus Bin. *Design and Prototyping a Peristaltic Pump*. Malaysia, 2008. Bachelor's thesis. University of Malaysia Pahang.

[17] DHUMAT, Suhas R. Design and Development of Rotary Peristaltic Pump. *International Journal of Science and Advanced Technology*. 2012, (2), 1-7. ISSN 2221-8386.

[18] How a Peristaltic Pump works. In: *Https://www.michael-smith-engineers.co.uk* [online]. Michael Smith Engineers [cit. 2019-05-20]. Available from: https://www.michael-smith-engineers.co.uk/mse/uploads/resources/literature/Ismatec/How-a-Peristaltic-Pump-Works.pdf

[19] BERG, Jordan M. a Tim DALLAS. Peristaltic Pumps. *Encyclopedia of Microfluidics and Nanofluidics*. Boston, MA: Springer US, 2013, 2013-4-20, , 1-12. DOI: 10.1007/978-3-642-27758-0_1198-2. ISBN 978-3-642-27758-0. Available: http://link.springer.com/10.1007/978-3-642-27758-0_1198-2

[20] ČÁPOVÁ, L. Vířivé čerpadlo, jako náhrada umělého srdce. Brno: Vysoké učení technické v Brně, Fakulta strojního inženýrství, 2018. 85 s. Vedoucí diplomové práce prof. Ing. František Pochylý, CSc..

[21] DRUKKER, William, Frank M. PARSONS a John F. MAHER. *Replacement of renal function by dialysis: a textbook of dialysis*. 2nd ed. Hingham, MA: distributors for the U.S. and Canada, Kluwer Boston, 1983. ISBN 08-983-8553-9.

[22] RUDOLF, Pavel. *Inovace peristaltického čerpadla pro mimotělní oběh omezující poškození červených krvinek (FP 390030): ZÁVĚREČNÁ ZPRÁVA GRANTU*. Brno

[23] NOON, George P., Larry E. KANE, Louis FELDMAN, Julia A. PETERSON a Michael E. DEBAKEY. Reduction of blood trauma in roller pumps for long-term perfusion. *World Journal of Surgery*. 1985, **9**(1), 65-71. DOI: 10.1007/BF01656257. ISSN 0364-2313. Available from: http://link.springer.com/10.1007/BF01656257

[24] DOLNÍČEK, P. *Stanovení dynamických vlastností zpětného ventilu*. Brno University of Technology, Faculty of Mechanical Engineering, 2017. 65 s. Supervisor Ing. Daniel Himr, Ph.D..

[25] POCHYLÝ, F. Lectures on Fluid structure interaction. Brno University of Technology, 2019.

[26] CENGEL, Yunus A. a John M. CIMBALA. Fluid mechanics: fundamentals and applications. 2nd ed. Boston: McGraw-Hill Higher Education, c2010. ISBN 00-772-9546-3.

[27] DANČÁK, Z. *Teoreticko-experimentální stanovení měrné energie vířivého čerpadla*. Brno University of Technology, Faculty of Mechanical Engineering, 2011. 68 s. Supervisor Ing. Simona Fialová, Ph.D.

[28] POCHYLÝ, F. Dynamika tekutinových systémů. Brno University of Technology, 1990. ISBN 80-214-0139-7.

[29] GABUTTI, Luca, Giuseppe COLUCCI, Antonio MARTELLA, Carlo SCHÖNHOLZER a Claudio MARONE. Does Monitoring of Pre-/Post-Dialyzer Pressure Difference Improve Efficiency in Intermittent Hemodialysis?. *Blood Purification*. 2003, **21**(4-5), 294-300. DOI: 10.1159/000072548. Available from: https://www.karger.com/Article/FullText/72548

[30] SHI, Mei Qiong. *Deformation of Rubber Membranes Subjected to Fluid Loading*. Canada, 2009. Master's Thesis. McGill University, Montréal.

[31] *Email communication with Ing. Dominik Šedivý*. Brno, 2019.

[32] *Email communication with prof. Ing. Jiří Burša, Ph.D.*, Brno, 2019

[33] RUDOLF, P. Lectures on Computational fluid dynamics. Brno University of Technology, 2019.

[34] *ANSYS FLUENT: Manual* [online]. [cit. 2019-05-23]. Dostupné z: https://www.sharcnet.ca/Software/Fluent6/html/udf/node78.ht m

[35] *ANSYS FLUENT: Manual* [online]. [cit. 2019-05-23]. Dostupné z: https://www.sharcnet.ca/Software/Ansys/16.2.3/enus/help/flu_ug/flu_ug_dynam_mesh_update.html#x1-94200012.3.2

[36] *ANSYS FLUENT: Manual* [online]. [cit. 2019-05-23]. Dostupné z: https://www.sharcnet.ca/Software/Ansys/16.2.3/enus/help/flu_ug/flu_ug_dynam_mesh_update.html#flu_ug_remesh_meth

[37] *ANSYS FLUENT: Manual* [online]. [cit. 2019-05-23]. Dostupné z: https://www.sharcnet.ca/Software/Fluent6/html/udf/node96.htm

List of symbols and abbreviations

Variable	Unit	Definition
2D		Two-Dimensional
3D		Three-Dimensional
ABS		Plastic material: Acrylonitrile-Butadiene-Styrene
AV		Arteriovenous fistula
CFD		Computational fluid dynamics
ESKD		End stage kidney disease
FSI		Fluid Structure Interaction
k-ε		Turbulence model k-ε
Ms		Microsoft
RANS		Reynolds averaged Navier-Stokes equations
RPM		Revolutions per minute
RPS		Revolutions per second
UDF		User Defined Function
UDMI		User Defined Memory
b	[Pas]	Second viscosity
C	[-]	Control point for wall deformation
d_{roller}	[m]	Diameter of the roller
d_{tube}	[m]	Inner diameter of the tube
D	[m]	Diameter of casing
D_{tube}	[m]	Outer diameter of the tube
E	[Pa]	Young's modulus
F_d	[N]	Deformation force
F_i	[N]	Force vector
g_i	[ms^{-2}]	Vector of gravitational acceleration
G	[Pa]	Linear elastic modulus
I_1	[-]	First principal invariant
i, j, k	[-]	Index
k	[Jkg^{-1}]	Boltzman's constant
l_{180}	[m]	Length between rollers
l_{R-r}	[m]	Length between the center of rotation and tygon tube
L	[m]	Length of tube
m_j	[-]	Normal unit vector
Mk_c	[Nm]	Total toque
M_{kd}	[Nm]	Deformation torque
n	[min^{-1}]	Revolution per minute
n_j	[-]	Normal unit vector
N	[-]	Number of chains of molecules per unit volume

Variable	Unit	Definition
N_{roller}	[-]	Number of rollers
N_{sup}	[-]	Number of support roller
p	[Pa]	Pressure
Δp	[Pa]	Pressure difference
p_2	[Pa]	Pressure behind the pump
p_3	[Pa]	Pressure behind the dialyzer
$p_{dialyzer}$	[Pa]	Pressure drop on the dialyzer
P_C	[W]	Total power
P_d	[W]	Deformation power
P_e	[W]	Power from experiment
P_h	[W]	Hydraulic power
O_c	[-]	Occlusion
Q	[m^3s^{-1}]	Flow rate
Q_{const}	[m^3s^{-1}]	Flow rate during constant movement from simulations
Q_{mean}	[m^3s^{-1}]	Mean flow rate obtained simulations
Q_{th}	[m^3s^{-1}]	Theoretical flow rate
r	[m]	Radius of inner wall of the tube
R	[m]	Radius inner casing
R_r	[m]	Distance between center of rotation and center of roller
R_{sup}	[m]	Radius of support roller
s	[m]	Occlusion gap
S	[m^2]	Deforming surface
S_1	[m^2]	Inlet surface
S_2	[m^2]	Outlet surface
S_{tube}	[m^2]	Cross section of the tube
t	[s]	Time
t	[m]	Thickness of the wall
T	[K]	Absolute temperature
u_B	[-]	Type B uncertainty
v_i, v_j	[ms^{-1}]	Vector of velocity
v_{ij}	[s^{-1}]	Rate-of-stain tensor
v_{kk}	[s^{-1}]	Divergence of velocity
v_n	[ms^{-1}]	Normal vector of velocity
V	[m^3]	Volume
V_g	[m^3]	Volume between rollers
W	[J]	Energy stored in tygon tube
x_i, x_j, x_j	[m]	Vector of dimension
ΔY	[Jkg^{-1}]	Hydraulic energy

Variable	Unit	Definition
Γ	[m^2]	Steady wall surface
δ_{ij}	[-]	Kronecker tensor
η	[-]	Efficiency from experiment
η	[Pas]	Dynamic viscosity
η_{est}	[-]	Estimated efficiency
θ	[m^2]	Union of surfaces
$\lambda_1, \lambda_2, \lambda_3$	[-]	Principal stretch ratios
μ	[m^2s]	Kinematic viscosity
μ	[-]	Poisson's ratio
π	[-]	Ludolph's number
π_{ij}	[Pa]	Viscous stress tensor
ρ	[m^3kg^{-1}]	Density
σ_{ij}	[Pa]	Stress tensor
ω	[s^{-1}]	Angular velocity
ω_j	[s^{-1}]	Vector of vorticity
τ_{ij}	[Pa]	Tensor of mechanical pressure

List of figures

List of appendices

Appendix 1 – CD

- UDF for peristaltic pump movement
- Examples of Excel evaluation
- Designs
- Photos of the circuits

Appendix 2 – Prove of simplifications used for derivation of force from Navier-Stokes equations

Appendix 1

See enclosed CD.

Appendix 2 – Prove of simplifications used for derivation of force from Navier-Stokes equations

$$g_i = \frac{\partial}{\partial x_j}\left(\delta_{ij} g_l x_l\right) = \delta_{ij} g_l \frac{\partial x_l}{\partial x_j} = \delta_{ij} g_l \delta_{jl} = g_i$$

$$\frac{\partial v_i}{\partial x_j} v_j = \frac{\partial}{\partial x_j}\left(v_i v_j\right) = \frac{\partial v_i}{\partial x_j} v_j + \frac{\partial v_j}{\partial x_j} v_i = \frac{\partial v_i}{\partial x_j} v_j$$

$$\frac{\partial v_i}{\partial t} = \frac{\partial}{\partial x_j}\left(\frac{\partial v_j}{\partial t} x_i\right) = \frac{\partial^2 v_j}{\partial x_j \partial t} + \frac{\partial v_j}{\partial t}\frac{\partial x_i}{\partial x_j} = \frac{\partial v_j}{\partial t}\delta_{ij} = \frac{\partial v_i}{\partial t}$$